TU Wien
Institute of Atomic and Subatomic Physics

Project Work

within the bachelor degree course of technical physics

Title: Simulation of superconducting thin films

Author: Schernthaner Klara, MatNr. e1326189
(klara_schernthaner@hotmail.com)
Rabensteiner Alexander, MatNr. e1327097
(pietracorvo@hotmail.com)

Version from: April 8, 2019

Supervised by: Prof. Dr. Jörg Schmiedmayer
Dr. Stefan Minniberger
Dr. Fritz R. Diorico

Abstract

Within this thesis the simulation of superconducting thin films in the Meissner state is treated.
The calculation of the current distribution of a hard type-II superconductors in the Meissner phase is carried out within the London approximation and implemented by an energy minimization approach. Beside the discussion of the theoretical fundamentals of superconductivity, calculations of generic geometries and boundary conditions were carried out. The concrete implementation follows the procedure proposed by Sanchez et al. ([1] and [2]). Furthermore, an optimization of the algorithm was accomplished by implementing an energy difference method which reduces the computation time significantly.
Different cases of superconductors subjected to either external feeding currents I_a or external magnetic fields H_a are described. The resulting current distribution as well as the corresponding magnetic fields are discussed.
Furthermore, the effect of different geometries on the current distributions and the resulting magnetic fields is treated. These geometries consist of the straight strip, the $\frac{\pi}{2}$-turn, the strip with a hole and an isolated superconductor.
Calculations were carried out on grids with a size of 50×50 points, for most geometries more than 100.000 iterations have been applied.

Zusammenfassung

Inhalt dieser Arbeit stellt die Simulation supraleitender Dünnfilme in der Meissner Phase dar.
Die Berechnung der Stromverteilung eines Typ II Supraleiters in der Meissner Phase wird im Rahmen der London Näherung duchgeführt und mittels eines Variationsansatzes für die Gesamtenergie der Magnetisierung implementiert. Neben der Behandlung des theoretischen Fundaments zur Supraleitung, wurden Berechnungen für generische Geometrien und Randbedingungne ausgeführt. Die praktische Implementierung folgt der Vorgehensweise vorgeschlagen von Sanchez et al. ([1] and [2]). Im Zuge der Durchführung konnte die Rechenzeit des Algorithmus mtihilfe einer Energiedifferenz Methode signifikant reduzierzt werden.
Verschiedene Fälle von Supraleitern unter angelegtem externem Strom I_a oder externem Magnetfeld H_a wurden behandelt, die resultierende Stromverteilung sowie das generierte Magnetfeld wurden untersucht.
Im Weiteren wurde der Einfluss verschiedener Geometrien auf die Stromverteilung und das resultierende Magnetfeld analysiert. Die behandelten Geometrien umfassen den geraden Leiter (strip) die $\frac{\pi}{2}$ Kurve, den geraden Leiter mit Loch und ein Stück isolierten Supraleiter (island).
Alle Berechnugnen wurden auf einem Gitter mit 50×50 Punkten ausgeführt, für die meisten Geometrien wurden rund 100.000 Iterationsschritte ausgeführt.

Contents

List of Figures

1 Introduction

Thin film superconductors provide a wide field of application in experimental physics. Mainly the generation of magnetical microtraps to collect a significant number of Bose-Einstein condensated atoms in potential minimums just above the conductor seems to be a promising method, with applications such as simulation of solid state physics or the construction of 'quantum memory' to store highly correlated quantum states.
In a novel experiment at the AI Vienna a big number of laser cooled ^{87}Rb atoms ($> 10^8$) shall be trapped above a sapphire substrate chip with a sputtered Niobium based hard type-II superconductor. The thickness of the superconducting film is about t $\approx$ 500nm and small compared to the width (W $\approx 10\mu$m) of the conducting tracks. The thin film approximation (homogeneous currents in vertical direction) is satisfied as long as the penetration depth λ is in the order of the thickness t. The current geometry of the superconductor used in the experiment to trap the atoms is the Z shape, where the atom cloud is trapped at the field minimum between the two 90° turns.
To achieve a better control of the atom cloud a deeper understanding of the behaviour of superconducting geometries is essential.
The aim of the following work is to provide a method, to calculate the magnetization, the current distribution and the resulting magnetic field of a superconducting atomic chip subjected to either an external field or current. This work includes only the simulation of the Meissner state, an implementation of the Bean critical model (which is a better approximation for the behaviour of Niobium based superconductors used in the experiment) shall be undertaken in future works.
The task to find the actual currents can be reduced to the calculation of the magnetization g(x,y). This is carried out by a brute force energy minimization approach: starting from an arbitrary magnetization, every value of the discretized matrix g(i,j) has to be variated by $\pm\Delta$g and the energy of the new magnetization g'(i,j) = g(i,j)$\pm\Delta$g is calculated. After the variation of every node the new energies are compared and the variation, minimizing the energy the most, is applied.
Calculations were performed on grids with 50×50 grid-points. Geometries tested in this thesis are the strip geometry, the $\frac{\pi}{2}$-turn, the strip with hole and an isolated superconductor.
The information of how different geometries, applied currents and applied magnetic fields change the current distribution of the sample will hopefully help to improve microtraps for ultracold atoms.

2 Theoretical background of superconductors

In this chapter, the fundamental properties of superconductors are discussed. Three models describing superconductors will be considered, as well as hysteresis in type II superconductors.

2.1 Properties

Superconductivity is the property of a material to transport current without resistance below a certain transition temperature T_c, as well as a perfect diamagnetic behavior. It can be roughly classified into two types of superconductors (SC), called type I and type II superconductor.

Type I superconductors have very low transition temperatures and are mostly metals (e.g. the critical temperature for mercury yielding to zero resistance is $T_c = 4.15$ K). Below T_c, the SC starts to suppress any external magnetic field B, trying to penetrate it, by establishing surface currents that induce a magnetization opposing the magnetic field. Inside the SC, the field vanishes completely. This effect is called Meissner effect. It is obtained, regardless if the superconducting phase is first established and then the magnetic field applied or vice versa. As a consequence, the superconducting state has to be a thermodynamic phase.

Exceeding T_c or a critical magnetic field B_c, the superconducting state brakes down and the normal conducting state is reestablished.

There are two equations successfully describing the Meissner state called the London equations. They will be described in section 2.2.1.

Another theory trying to explain the phenomena of superconductivity is the BCS-theory. It is very successful in describing type I superconductors, but fails to explain the mixed state in type II superconductors. It will be described in section 2.2.2.

Type II superconductors are mostly isolators or materials with high electrical resistance in their normal state. They have higher critical temperatures than type I superconductors (until now the highest transition temperature of a type II SC is $T_c = 138K$) and two critical fields B_{c_1} and B_{c_2}. Below B_{c_1}, they behave like type I SC, establishing the Meissner state.

Exceeding B_{c_1} the superconductor enters a mixed state, where the magnetic field B starts to penetrate it through quantized vortices called Abrikosov vortices (fig.1). These normal conducting vortices are shielded by supercurrents inside the SC, making sure that the space between two vortices is still field-free. Increasing B, more vortices start to penetrate the superconductor, they start to grow and the space between them gets smaller until B_{c_2} is reached and the superconducting state dissolves.

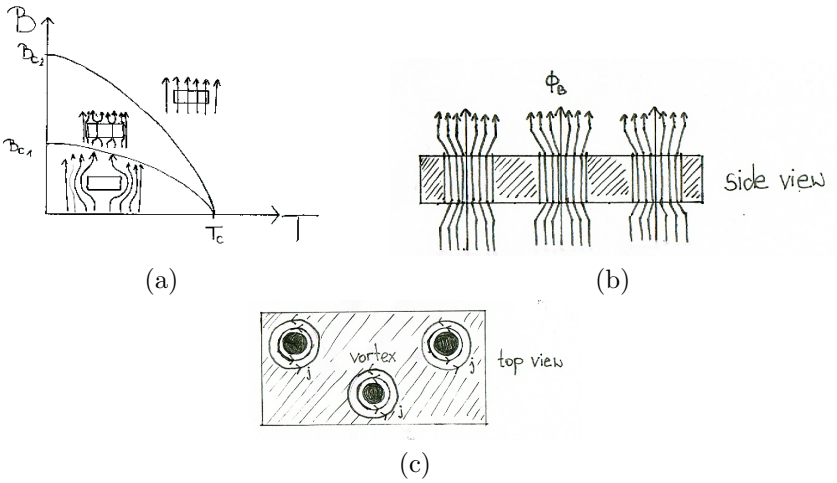

Figure 1: (a) Phase diagram of a type II superconductor. Below B_{c_1} the magnetic field B is expelled completely. Between B_{c_1} and B_{c_2} the field starts to penetrate the SC through quantized vortices. (b) side view of the magnetic flux Φ_B passing through the SC (c) top view of Abrikosov vortices penetrating the superconductor with the supercurrents circulating around the normal conducting part.

A consequence of the penetration is hysteretic behavior which can be observed in the mixed state in type II superconductors (cf. section 2.3).
Aside from the critical temperature T_c and the critical field B_c, there is a third limiting factor that terminates the superconducting state. If a critical current I_c is fed into the SC, the superconducting state also brakes down. These critical currents can be increased in type II SC, by doping the SC. This is very interesting for superconducting technology since not only high magnetic fields, but also high supercurrents, are of great interest. The critical current, as well as the doping of superconductors play an important role for the hysteresis in type II superconductors and are therefore also discussed in section 2.3.
An important theory that describes the Meissner state, as well as the mixed state, is the Ginzburg-Landau-Theory described in section 2.2.3.

2.2 Models describing superconductivity

2.2.1 London equations

The London equations were the first equations to successfully describe the superconducting properties.

$$\partial_t \mathbf{j} = \frac{n_s \cdot q_s^2}{m_s} \mathbf{E} \tag{1}$$

is called the 1. London equation. It replaces Ohm's law $\mathbf{j} = \sigma\mathbf{E}$ which only applies to normal conductors, where $\rho \neq 0$. The factor $\frac{m_s}{n_s \cdot q_s^2}$ is called the London parameter Λ, m_s is the mass of the superconducting particles, q_s is their charge, and n_s the density of the superconducting charge carriers.

$$\mathbf{j}_s = -\frac{n_s \cdot q_s^2}{m_s}\mathbf{A} \tag{2}$$

is the 2. London equation. It links the local current density $\mathbf{j}_s$ inside the superconductor directly to the local vector potential $\mathbf{A}$. Using the Maxwell equations, the 2. London equation can be rewritten as

$$\Delta\mathbf{B} = \frac{1}{\lambda_L^2}\mathbf{B} \tag{3}$$

where Δ is the Laplacian, $\mathbf{B}$ the external magnetic field and

$$\lambda_L = \sqrt{\frac{m_s}{\mu_0 n_s q_s^2}} \tag{4}$$

the London penetration depth. λ is the characteristic length for the exponential decay of the field in the superconductor, since the solution of Eq.(3) is $B_z(x) = B_z(0)exp(\frac{-x}{\lambda_L})$. This means, that the external field is not completely expelled from the superconductor. There is still a small layer where the field penetrates it. The currents, responsible of shielding the field, circulate within this layer.
In case of thin film superconductors, where the thickness of the sample is smaller than the London penetration depth, this means that the current density is constant along its thickness. This will be very useful for the calculation method presented in chapter 3.

2.2.2 BCS Theory

The BCS Theory (Bardeen, Cooper and Schrieffer) is based on the assumption, that the electrons of a metal form pairs, called cooper pairs. This happens via an electron-electron interaction. Only electrons that have opposite spins and opposite momenta (with $\mathbf{p} = \hbar\mathbf{k}$) form cooper pairs $\{\mathbf{k}\uparrow, -\mathbf{k}\downarrow\}$.
The main consequence of this coupling is, that a cooper pair has an integer spin and, for that reason, is not restricted to the Pauli exclusion principle. These pairs can therefore occupy the same ground state which has a lower energy level. Hence, it is energetically favorable to form these pairs.
The energy difference that emerges when single electrons form cooper pairs is called condensation energy Δ. This energy gap has to be overcome in order to break the cooper pairs and with that the superconducting state.

2.2.3 Ginzburg-Landau-Theory

The Ginzburg-Landau-Theory describes type I and type II superconductors by using thermodynamic considerations.
It is an extension of the London equations, which consider a constant spacial density of the superconducting charge carriers, and therefore can not describe the mixed state in type II SC. The assumption of the constant spacial density is no longer given, because of the vortices starting to penetrate the SC by breaking cooper pairs. By considering that, the Ginzburg-Landau-Theory achieves to describe the Meissner state, as well as the mixed state.
According to this theory, the change from the normal conducting state to the superconducting state constitutes a second-order phase transition and can therefore be calculated using the Landau-theory [7, 8].
The macroscopic wave function Ψ, describing the superconducting state, is chosen as the order parameter. It is related to the density of the superconducting charge carriers n_s by

$$|\Psi|^2 = |\Psi_0|^2 = n_s \tag{5}$$

The choice of the wave function Ψ as the order parameter is motivated by the fact that it should steadily grow from zero at $T = T_c$, to one at $T = 0$. This is achieved with the relation described by Eq.(5). There are no cooper pairs above the transition temperature but decreasing the temperature, its density increases as more and more electrons combine to cooper pairs.
Because the order parameter is very small at temperatures close to the transition temperature, the Gibbs function describing the superconducting state can be approximated at these temperatures by its taylor series

$$g_s = g_n + \alpha|\Psi|^2 + \frac{1}{2}\beta|\Psi|^4 + ... \tag{6}$$

where g_s is the superconducting and g_n the normal conducting Gibbs function. The fact that there are only even exponents derives from the Landau-theory of second order phase transitions [7].
Eq.(6) however, does not constitute for the energy of the local field expulsion, nor for the spacial variation of Ψ, which can be observed in the Mixed state of superconductors.
In order to correct that, the term obtained by the Landau-Theory, has to be expanded by two terms. It is the important difference between the Landau-Theory and the Ginzburg-Landau Theory and leads to

$$g_s(B) = g_n + \alpha|\Psi|^2 + \frac{1}{2}\beta|\Psi|^4 + \frac{1}{2\mu_0}|\mathbf{B}_0 - \mathbf{B}_i|^2 + \frac{1}{2m}\left|\left(\frac{\hbar}{i}\nabla - q\mathbf{A}\right)\Psi\right|^2 \tag{7}$$

where $\mathbf{B}_0$ is the magnetic field outside, $\mathbf{B}_i$ the magnetic field inside the SC, ∇ the nabla symbol and $\mathbf{A}$ the magnetic vector potential. With $\mathbf{p} = -i\hbar\nabla$, the

expression in the parenthesis in the last term stands for the generalized momentum $\mathbf{p} - q\mathbf{A}$. In this equation, the first three terms stand for the Landau theory.
The fourth term accounts for the energy that is needed to suppress/lower the external magnetic field inside the superconductor. In case of the Meissner state, where $\mathbf{B}_i = 0$, this term has the highest value.
The last term holds information about variations of Ψ and $\mathbf{B}_i$ and therefore accounts for the interfacial energy between the normal conducting and superconducting state.
In order to obtain the Ginzburg-Landau equations the Gibbs function of the SC has to be minimized. This leads to two equations. By variating Ψ, the first Ginzburg-Landau equation is obtained

$$\frac{1}{2m}\Big(\frac{\hbar}{i}\nabla - q\mathbf{A}\Big)^2\Psi + \alpha\Psi + \beta|\Psi|^2\Psi = 0 \tag{8}$$

Variating $\mathbf{A}$ yields to the second Ginzburg-Landau equation

$$\mathbf{j}_s = \frac{q\hbar}{2mi}(\Psi^*\nabla\Psi - \Psi\nabla\Psi^*) - \frac{q^2}{m}|\Psi|^2\mathbf{A} \tag{9}$$

with Ψ^* being the komplex function of Ψ. Eq. (9) is an expansion of the second London equation (2), as it depicts the density of the supercurrent at every point inside the inhomogeneous SC.
It also holds information about any normal conducting parts inside the SC and therefore, describes the fluxons entering the SC. As mentioned before, the magnetic field, which is continuous outside the SC, enters the probe trough these fluxons, with the smallest magnetic flux quantum given by

$$\Phi_0 = \frac{h}{2e} = 2.07 \cdot 10^{-15} Wb \tag{10}$$

The fact that there is two times the electron charge in the denominator can be seen as prove of the existence of cooper pairs.
According to the Ginzburg-Landau theory, the superconducting phase has two characteristic lengths, namely the Ginzburg-Landau coherence length ξ_{GL} and the London penetration depth λ_L (fig.2). The Ginzburg-Landau coherence length can be derived from Eq.(8) [8]. Using $\psi(x) = \Psi(x)/\Psi_0$ and $|\Psi_0|^2 = n_s = -\alpha/\beta$ it can be written as

$$-\xi_{GL}^2(\frac{1}{i}\nabla - \frac{q}{\hbar}\mathbf{A})^2\psi + \psi - |\psi|^2\psi = 0 \tag{11}$$

with ξ_{GL} being

$$\xi_{GL} = \frac{\hbar}{\sqrt{2m_s|\alpha|}} \tag{12}$$

It characterizes the scale in which the order parameter Ψ changes at a disturbance within the SC. Hence, it describes the dimensions of the vortices. It also depicts the change of Ψ at the surface of the superconductor.
The London penetration depth characterizes the length of the exponential decay of an external field penetrating the superconductor and was first described in the London equations (cf. 2.2.1). The difference to Eq.(4) is that the density of the cooper pairs is no longer stable and therefore has to be modified by $n_s = 4|\Psi(x)|^2$, in order to account for their local dependence. Hence, the London penetration depth according to the Ginzburg-Landau theory changes to

$$\lambda_L = \sqrt{\frac{m_s}{4\mu_0|\Psi(x)|^2 q_s^2}} \tag{13}$$

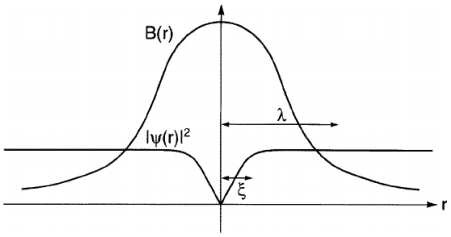

Figure 2: Scheme of a vortex in a type II SC. ξ is the coherence length of the order parameter. λ is the London penetration depth.

The ratio between the London penetration depth λ_L and the Ginzburg-Landau coherence length ξ_{GL} is called the Ginzburg-Landau parameter κ.

$$\kappa = \frac{\lambda_L}{\xi_{GL}} \tag{14}$$

It is independent regarding the temperature and the magnetic field and can be used to classify superconductors into type I and type II superconductors.
If $\kappa < \frac{1}{\sqrt{2}}$, the surface energy is greater than zero and the SC constitutes a type I superconductor.
If $\kappa > \frac{1}{\sqrt{2}}$, the surface energy is smaller than zero and the SC constitutes a type II superconductor.
Using the Landau equations, the critical fields B_{c1} and B_{c2} can be calculated [7]. For B_{c1} this yields to $B_{c1} \simeq \frac{\Psi_0}{4\pi\lambda^2} \ln\kappa$. The London penetration depth can be found in the denominator of the formula. Knowing the first critical field is therefore a good indicator to estimate the London penetration depth for a specific sample.
The second critical field B_{c2} can be calculated using $B_{c2} \simeq \frac{\Psi_0}{2\pi\xi^2}$. The Ginzburg-Landau corherence length in the dominator can be understood, considering that the second critical field is reached, when the distance between the fluxons is of

the order of ξ_{GL}. Again, knowing B_{c2}, one can estimate the Ginzburg-Landau coherence length. In order to find the critical fields, the magnetization curve can be taken into consideration, as $\mathbf{M}(\mathbf{B})$ and the critical fields are strongly correlated (cf. 2.3).

2.3 Hysteresis in type II superconductors

2.3.1 Magnetization of superconductors

The magnetization curves $\mathbf{M}(\mathbf{B})$ of type I and type II superconductors illustrate the difference between them (cf. 3).
In type I superconductors, when exposed to an external magnetic field $B < B_c$, the magnetization linearly grows from zero until reaching its highest value at $B = B_c$. Exceeding B_c, $M(B)$ abruptly falls back to zero, as the superconducting state breaks down. This behavior is expected, as the superconductor depicts a perfect diamagnet.
In type II superconductors, the magnetization curve also starts from zero and linearly grows until the first critical field B_{c_1} is reached. At this point $\mathbf{B}$ starts to penetrate the SC and the probe enters the Shubnikov phase. With every fluxon that enters the probe, the magnetization decreases until reaching zero at B_{c_2}.

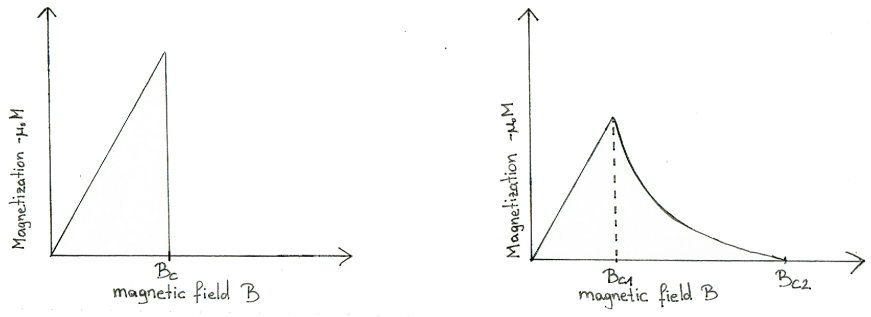

Figure 3: left: Ideal magnetization curve of a type I superconductor. $|\mathbf{M}(B)|$ linearly grows until reaching B_c. Exceeding B_c the Magnetization abruptly falls back to zero as the superconducting state breaks down. right: Ideal magnetization curve of a type II superconductor. Below B_{c1} behaves like a type I superconductor. Between B_{c1} and B_{c2} the magnetic field starts to penetrate the superconductor through quantized vortices.

This kind of magnetization curve however, only applies to perfect type II superconductors, with very little impurities, as can bee seen with the following example. Consider a planar type II SC subjected to an external field $|\mathbf{B}_z|$ and a stream current $|\mathbf{I}_x|$. As the SC enters the mixed state, the fluxons start to interact with

the current and, as a result, the Lorentz force $|\mathbf{F}_y| = q \cdot (|\mathbf{v}_x| \times |\mathbf{B}_z|)$ acts on them. This provokes a movement of the flux lines, in this case in y-direction, called flux creep (fig4).

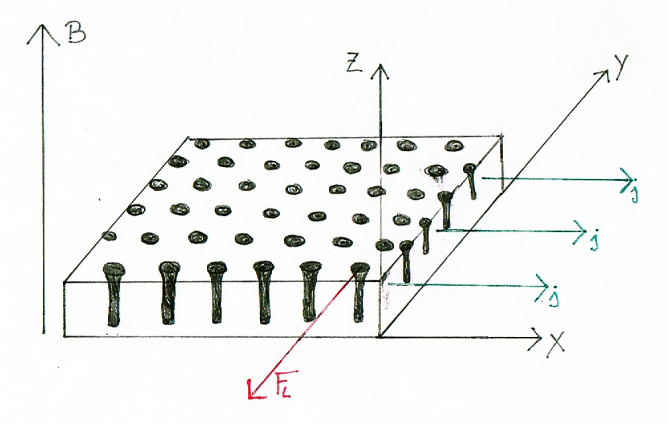

Figure 4: Scheme of a superconductor subjected to an external applied field and current $I = j \cdot A$. The Lorentz force $F_L = I \cdot L \cdot B$ acts on the vortices penetrating the sample and they start to move into the y-direction.

As the fluxon passes through the SC it induces electric fields. These fields accelerate the single electrons inside the probe. The resulting collision of the electrons with phonons provokes a dissipation of heat and eventually leads to the termination of the superconducting state.
According to the Lorentz force $|\mathbf{F}| = |\mathrm{I}| \cdot L \cdot |\mathbf{B}|$ for a current-carrying wire, even small currents provoke a movement and with that the termination of the superconducting state. For that reason, perfect superconductors are usually not suitable for technical realizations, where high transport currents are of great interest.
In order to avoid flux creep, hard superconductors can be used. Hard SC are probes that have been doped, similar to the doping of semi-conductors. The aim of doping the SC is to create a force, that opposes the Lorentz force and detain the flux lines from moving. A way to do so, is to place defected spots into the sample. Every impurity or inhomogeneity can act as such a spot as long as it is less favorable to superconductivity. These spots stay normal conducting while the rest of the probe enters the superconducting state at a certain temperature T_c.
Although it is energetically favorable to let the magnetic field penetrate the SC instead of shielding the whole sample, it is still very energy-intensive to create and shield a fluxon. The energy per length ϵ^* of a single fluxon is given by $\epsilon^* = B_{c1} \frac{\phi_0}{\mu_0}$ [8, 7, 6].
By creating normal conducting spots, the vortices have the possibility to reduce their length by going through these spots. As a consequence the energy is reduced

by $\epsilon^* \cdot l$. This means that the force of the pinning centers F_p is equivalent to the reduced energy per the length of the fluxon $F_p = \epsilon^* \cdot \frac{l}{x}$
Consequently, the external current that can be fed into the SC can be increased as long as $F_L < F_p$. Furthermore, it influences highly the magnetization of the probe, as $M(B)$ can not establish an equilibrium state as long a the vortices are pinned to their spots. Hence, a hysteretic behavior can be observed.
C.P. Bean used this behaviour to come up with a model that exploits the hysteresis curve of specific materials in order to calculate their current density. It will be discussed in the following section.

2.3.2 Bean critical state model

The Bean critical state model, as mentioned before, provides a model to link the magnetization of superconductors to the critical current density j_c. This is very useful, as the magnetization can be determined through experiments, while the critical current density is often hard to measure directly. This is due to the fact that j_c can get very high (up to 100A and more).
For his model Bean considered a hard type II superconducting hollow cylinder subjected to an external applied current $I = \mathbf{j} \cdot \mathbf{A}$. Once an external field $B < B_{c1}$ is applied, the SC shields the interior of the sample via supercurrents circulating within the London penetration depth. Once the field exceeds B_{c1} it enters the probe through Abrikosov vortices. These vortices are pinned to the defected spots in the SC and therefore enter the SC through them. Bean made the assumption, that the supercurrent density j_c is homogeneous and constant within the layer in which the fluxons penetrate the sample. This state, in which the current density and the magnetic field hold each other in balance is called the critical state and $\mathbf{j}_c$ the corresponding critical current density [5, 6].
Once the external field is increased, the vortices move further into the sample until again, reaching the critical state with the same critical current density $\mathbf{j}_c$. Hence, the supercurrent grows proportionally with the thickness d.
Reaching the second critical field B_{c2}, the fluxons penetrate the hole sample and the critical current flows within the entire probe. However, there is no magnetic field inside the void of the rod. Only when increasing the magnetic field above B_{c2} it reaches the interior of the probe (fig 5).
Decreasing the external field B_e again provokes a change of the supercurrents shielding the probe and the fluxons appear to be growing out of the superconductor. Decreasing the external field further provokes a reduction of the field inside the cylinder, until reaching a certain value at $B_e = 0$. Only when the external field reaches B_{c2}, the field within the cylinder equals zero.
In case of the hollow rod the relation between the magnetization curve and the critical current density can be calculated as follows.

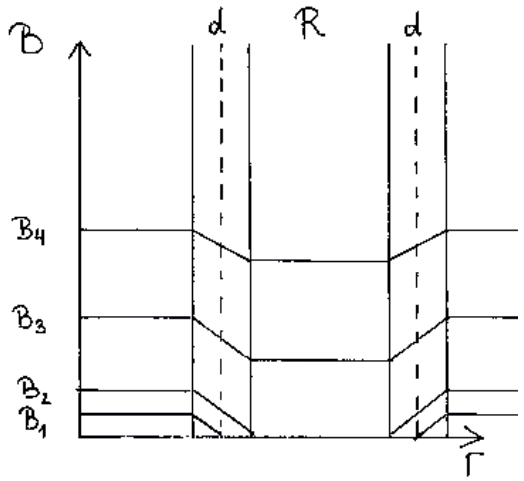

Figure 5: Scheme of a hollow cylinder. B_1 entered the probe until reaching the critical state in the middle of the cylinders wall. B_2 penetrates the hole sample, but does not reach the inside of the rod. Only when increasing the external field further it enters the void.

Using Ampere's law yields the link between $\mathbf{B}$ and $\mathbf{j}_c$: $\oint \mathbf{B} d\mathbf{S} = \mu_0 I = \mu_0 \cdot \mathbf{j}_c \cdot \mathbf{A}$, and therefore $B \cdot L = \mu_0 \cdot \mathbf{j}_c \cdot L \cdot d$, with $\mathbf{A}$ being the cross-section area of the rod's wall and $\mathbf{d}$ being its diameter.
The relationship $\mathbf{B} = \mu_0(\mathbf{H}+\mathbf{M})$ can be written as $M = \frac{B_i - B_o}{\mu_0}$ with the assumption that $\mathbf{M}$ is zero before applying the external field, $\mathbf{B}_i$ being the field inside the probe and $\mathbf{B}_e$ the field on the otside.
Combining the these two equations yields $|\mathbf{M}| = j_c \cdot d \cdot$ and with that the desired link between the magnetization and the critical current density.

3 Calculation method

This chapter provides a theoretical overview of how the implementation of the calculation method is done. In section 3.1 the calculation method will be discussed within the Meissner state. The adaptation to the mixed state will be described in section 3.2. An explanation of the actual implementation of the algorithm will be given in chapter 4.

3.1 Meissner state

The calculation method is based on an optimization problem with the objective to find the minimum of an energy function and the corresponding stream function within a superconducting atom chip. In this thesis only planar thin film superconductors that are thinner than the London penetration depth are considered. As a consequence, the current density $\mathbf{J}(x, y)$ is constant along the thickness d of the superconductor. Hence, the sheet current $\mathbf{K}(x, y)$ can be used. It is obtained by integrating the current density over the thickness d. Assuming that the midplane of the sample is at $z = 0$ one receives $\mathbf{K}(x, y)$ by $K = \int_{-d/2}^{d/2} \mathbf{J}(x, y, z)dz \simeq \mathbf{J}(x, y, 0) \cdot d$. The sheet current depends on a few key factors. These include the special geometry of the sample, intrinsic properties of the superconductor and external influences like applied magnetic fields and currents. It is assumed that there is either a longitudinal transport current, a perpendicular uniform applied field or both subjected to the superconductor. For different geometries the current distribution resulting from applying only currents, only magnetic fields as well as both currents and magnetic fields simultaneously were calculated (cf. chapter 5).
Considering the London approximation and assuming that the sheet current is constant it can be said that $\nabla \cdot \mathbf{K} = 0$. Typically, it is much more convenient to use a scalar stream function rather than a sheet current. Hence, a function g(x,y), analogous to the vector potential of the magnetic induction, is defined as

$$\mathbf{K}(x, y) = \nabla \times [g(x, y)\hat{\mathbf{z}}] \tag{15}$$

where $\hat{\mathbf{z}}$ is the unit vector along the z axis. With this definition the divergence of the sheet current always disappears.
The Gibbs free energy is given by

$$E = E_{int} \ + E_{kin} \ + E_{ext} \tag{16}$$

The components are calculated as follows:

$$E_{int} = \frac{1}{2} \int_S \mathbf{K}(\mathbf{r}) \cdot \mathbf{A}_K(\mathbf{r}) dS = \frac{\mu_0}{8\pi} \int_S \int_S \frac{\nabla g(\mathbf{r}) \cdot \nabla' g(\mathbf{r}')}{|\mathbf{r} - \mathbf{r}'|} dS dS' \tag{17}$$

is the internal energy wich derives from the interaction of the induced currents and the magnetic field created by themselves. $\mathbf{A}_K(r)$ is the magnetic vector potential of the induced currents, $\int_S dS$ the surface integral of the superconducting sample, μ the vacuum permeability and $\mathbf{r} = (x, y)$ the position of the two dimensional vector in the xy-plane.

$$E_{kin} = \frac{\mu_0 \Lambda}{2} \int_S [\mathbf{K}(\mathbf{r})]^2 dS = \frac{\mu_0 \Lambda}{2} \int_S [\nabla g(\mathbf{r})]^2 dS \tag{18}$$

is the kinetic energy that is generated by the charge carriers. Λ is the London penetration depth.

$$E_{ext} = \int_S \mathbf{K}(\mathbf{r}) \cdot \mathbf{A}_a(\mathbf{r}) dS = \mu_0 H_a \int_S g(\mathbf{r}) dS - \oint_{\partial S} g(\mathbf{r}) \mathbf{A}_a(\mathbf{r}) \cdot d\mathbf{l} \tag{19}$$

is the external energy resulting from the interaction between the currents and the external applied field. $\mathbf{A}_a(r)$ is the magnetic vector potential of the applied field and $\int_{\partial S} d\mathbf{l}$ the line integral along the outer contour ∂S.

The first step, in order to find the sheet current minimizing the Energy, is to divide the superconductor into a grid of equal rectangulars consisting of N nodes and k cells. The function g(x,y) is defined at each node $n = 1, ..., N$. Its gradients $\nabla \mathbf{g}$ are defined inside each cell and can be calculated by bilinear interpolation. For doing so, the four g_n values at the nodes of the corresponding cells are needed. Once they are found, the gradient can be calculated in x- and y-direction separately by applying the difference quotient in these directions.

$$\nabla \mathbf{g}(x) = \frac{1}{2} \cdot \frac{1}{\delta x} [(g_{ur} - g_{ul}) + (g_{lr} - g_{ll})] \tag{20}$$

and

$$\nabla \mathbf{g}(y) = \frac{1}{2} \cdot \frac{1}{\delta y} [(g_{ll} - g_{ul}) + (g_{lr} - g_{ur})] \tag{21}$$

with g_{ul} being the value of the node in the upper left, g_{ur} the upper right, g_{ll} the lower left and g_{lr} the lower right corner of one cell. Its gradients ∇g can be calculated by bilinear interpolation between the four g(x,y)-values at the corresponding nodes.

Before starting the optimization, g(x,y) has to be defined. Thus, it is essential to be familiar with the properties of the stream function, which are described in [3]. The important property for this work is, that the difference of g(x,y) between two points is the current that crosses any continuous line connecting these points. As a result, the total current crossing the superconductor can be simulated by setting $g = 0$ at all the nodes on one of the borders and $g = I_a$ at the nodes of the other

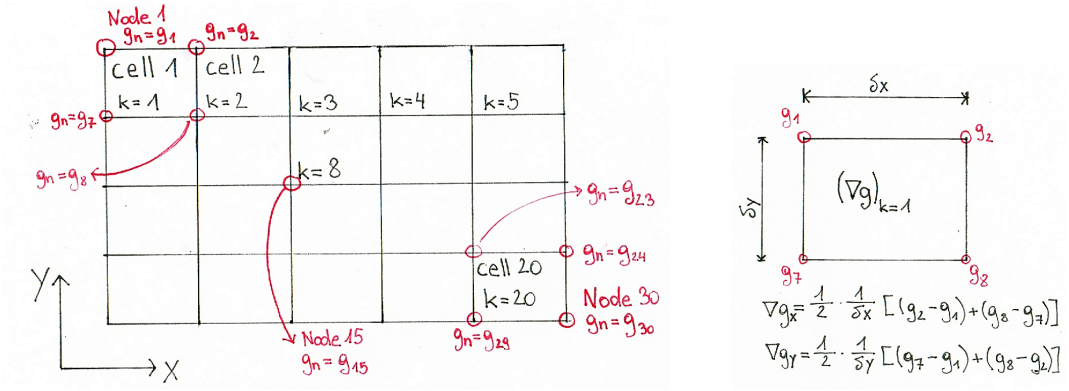

(a) (b)

Figure 6: (a) Superconducting sample divided into a grid of equal rectangulars consisting of N=1,..,30 Nodes and k=1,..,20 cells. The function g(x,y) is defined at each node $1, .., N$. (b) Calculation method for the gradient of a cell, in this case cell 1. ∇g can be calculated via the difference quotient in x-and y-direction

extreme. In case a hole is simulated, the nodes corresponding to it ought to have the same g value, making sure that no current is flowing inside the area. Knowing

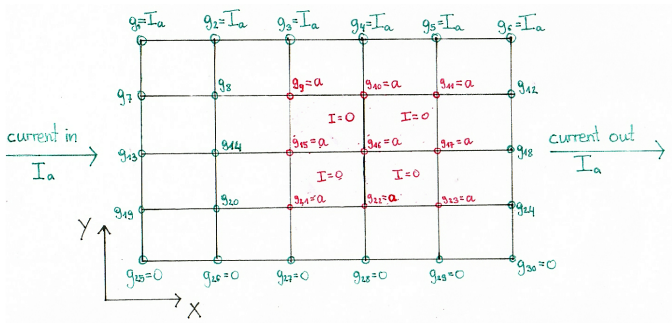

Figure 7: Superconducting sample with an external applied current. The total current is simulated by setting the borders I_a and 0 respectively. A hole is simulated by making sure that the g values corresponding to it have the same value.

this, the stream function can, in principle, be selected arbitrarily. However, it is convenient to start with a function close to the expected outcome (if known) since the calculation is very time-consuming. Also, g(x,y) has to be set according to the initial conditions imposed on the superconducting sample. Meaning that, if there is an external current fed into the superconductor, the borders have to be set $g = 0$ and $g = I_a$ accordingly. For the following procedure, there is also a numerical parameter $\Delta g > 0$ required. It should be set depending on the applied field and currents and, if needed, rescaled in order to be numerically accurate.

Once the g(x,y) function, and Δg are chosen the energy for the given distribution is calculated. Then, the g(x,y) value of the first node is modified with $\pm\Delta g$ and the energy recalculated. This process is repeated until every g(x,y), value has been modified. The node where the change of g(x,y) leads to the largest decrease of the energy is replaced by g(x,y) $\pm\Delta g$ and the whole process restarts and is repeated until there is no change in g(x,y) that leads to a decrease of E.

In order to implement the process, discretized expressions of the energies are required. To obtain them a matrix $G(x,y) = \nabla g(x,y)$ is defined. Inserting it in Eq.(17) yields

$$E_{int} \simeq \frac{\mu_0}{2} \int_S \int_{S'} \frac{\mathbf{G(x,y)} \cdot \mathbf{G(x',y')}}{|r - r'|} dS dS' \tag{22}$$

where $r = (x,y)$, $r' = (x',y')$, $dS = dxdy$ and $dS' = dx'dy'$ respectively. S and S' represent the surface of the superconductor. Since $G(x,y)$ is discrete and it is assumed to be constant inside the individual cells one can say that $G(x,y) \simeq G_k$ for all $(x,y) \in k$. This leads to

$$E_{int} \simeq \frac{\mu_0}{8\pi} \sum_{k,k'} \mathbf{G}_k \mathbf{G}_{k'} \int_{S_k} \int_{S_{k'}} \frac{dS' dS}{[(x-x')^2 + (y-y')^2]^{3/2}} \tag{23}$$

The double integral depends only on the geometry of the sample and the chosen dimensions of the grid. Therefore the magnitude $N_{k,k'}$ is defined as

$$N_{kk'} = \frac{1}{4\pi} \int_{S_k} \int_{S'_k} \left(\sqrt{(x-x')^2 + (y-y')^2} \right)^{-1} dS dS' \tag{24}$$

the values of $N_{k,k'}$ are symmetric regarding the k-indices and only depend on the relative positions of the cells k and k'. $N_{k,k'}$ is defined for general grids. In the case of rectangular cells an analytical expression is given in the appendix. [4] Thus the discretized internal energy results in

$$E_{int} \simeq \frac{\mu_0}{2} \sum_{k,k'} \mathbf{G}_k \cdot \mathbf{G}_{k'} N_{kk'} \tag{25}$$

Inserting G_k in Eq.(18) yields to the expression of the kinetic energy

$$E_{kin} \simeq \frac{\mu_0 \Lambda}{2} \sum_k (G_{k,x}^2 + G_{k,y}^2) \delta_x \delta_y \tag{26}$$

δ_x and δ_y are the dimensions of the cells in x- and y-direction respectively.

In order to calculate the external energy Eq.(19) can be simplified. The second term is relevant only for the cells defining the outer contours that are connected to the feeding cables. These cables are located far outside the region of interest and can thus be neglected. As mentioned above, g(x,y) is defined at each of the four nodes of one cell. The contribution of one cell to the energy is therefore proportional to the averaged value of the four g-values g_k^i. This leads to the discretized expression of the external energy.

$$E_{ext} \simeq \frac{\mu_0 \ H_a}{4} \sum_k \sum_{i=0}^{3} g_k^i \ \delta_x \ \delta_y \tag{27}$$

Using these expressions for the energies the g(x,y) distribution minimizing the Gibbs free energy within the superconductor can be calculated. Once the distribution is found, the sheet current K(x,y) can be estimated by using Eq.(15). The magnetic induction and the magnetic moment can be obtained directly from the g distribution. The z-component of the magnetic induction at z=0 can be calculated with

$$B_z \ (x,y) = \frac{\mu_0}{4\pi} \int_S \nabla' g(x',y') \cdot \nabla' \Big(\sqrt{(x-x')^2 + (y-y')^2} \Big) dx' dy' \tag{28}$$

3.2 Mixed state

Although the calculation method to find the g(x,y) distribution within the mixed state is based on the same procedure as in the Meissner state, there are crucial differences between these two states (cf. section 2.1). While the superconductor is completely shielded from any applied magnetic field (up to a critical field H_c) in the Meissner state, these fields start to penetrate the sample within the mixed state. This penetration leads to hysteresis of the superconductor. As a consequence, the total surface current is not allowed to exceed the surface critical current $\mathbf{K}_c = \mathbf{J}_c \cdot d$, in order to maintain the superconducting properties. The phenomena of hysteretic behavior within type II superconductors is described by the Bean critical state model (cf. section 2.3.2).

These differences are important for the way in which the g(x,y) function minimizing the energy is obtained. Other than in section 3.1 the energy function that is going to be minimized, has to contain information about the previous magnetic state [2].

It therefore changes to

$$\begin{aligned} F[g(r)] = & \frac{\mu_0}{8\pi}\int_S\int_S \frac{\nabla g(r)\cdot\nabla' g(r')}{|r-r'|}dSdS' \\ & - \frac{\mu_0}{4\pi}\int_S\int_S \frac{\nabla \hat{g}(r)\cdot\nabla' g(r')}{|r-r'|}dSdS' \\ & + \frac{\mu_0}{8\pi}\int_S\int_S \frac{\nabla \hat{g}(r)\cdot\nabla' \hat{g}(r')}{|r-r'|}dSdS' \\ & + \mu_0(H_a - \hat{H}_a)\int_S g(r)dS \\ & - \mu_0(H_a - \hat{H}_a)\int_S \hat{g}(r)dS \end{aligned} \tag{29}$$

Here, the first three terms come from the interaction of the induced currents and the magnetic field created by themselves and the last two terms represent the external energy resulting from the interaction between the currents and the external applied fields. The terms for the internal and external energy have been modified by $\hat{g}(r)$ and $\hat{\mathbf{H}}_a$ respectively. These variables are defined as

$$\hat{X} = X - \delta X \tag{30}$$

and hold the information about the previous magnetization of the sample. The quantity δX stands for the variation of X in case some of the external conditions vary and $\hat{X}$ for the amount of X before the change.
Comparing Eq.(17) from the Meissner state and the first three terms of Eq.(29) it becomes clear that the first term stays the same. It represents the 'new' internal energy, or to be more precise, the internal energy after a change in the external applied current.
The third term stands for the 'old' internal energy, or the energy before the change was applied. The second term is a mixed term
The last two terms in Eq.(29) stand for the external energy, again considering the change in the external applied field.
Inserting Eq.(30) into Eq.(29) yields to

$$F'[\delta g(r)] = \frac{\mu_0}{8\pi}\int_S\int_S \frac{\nabla \delta g(r)\cdot\nabla' \delta g(r')}{|r-r'|}dSdS' + \mu_0(\delta H_a)\int_S \delta g(r)dS \tag{31}$$

It is equivalent to minimize Eq.(31) instead of Eq.(29) in order to find the desired distribution g(x,y).
In order to obtain the discretized energyfunction the procedure is the same as in section 3.1. and yields to

$$F'[\delta g(r)] \;\simeq \frac{\mu_0}{2}\sum_{k,k'} \delta\mathbf{G}_k \;\cdot \delta\mathbf{G}_{k'}\; N_{kk'} \;+ \frac{\mu_0\;\delta H_a}{4}\sum_k\sum_{i=0}^{3} \delta g_k^i\;\delta_x\;\delta_y \tag{32}$$

Like in the previous section the superconductor is divided into a grid of rectangular cells consistent of N nodes and k cells. g(x,y) is defined at the nodes and the gradients ∇g are calculated by bilinear interpolation. Other than in the Meissner state, it is of great importance that the absolute values of the gradients are lower or equal than the surface critical current $\mathbf{K}_c = \mathbf{J}_c d$.
This constraint results from the mixed state in which the total surface current is not allowed to exceed the surface critical current in order to maintain the superconducting properties.
Again the scalar stream function corresponding to the minimum of Eq.(29) or Eq.(31) is obtained by varying the g values with $\pm\nabla g$ but with the restriction that only at the nodes, where all the neighboring cells satisfy the constraint $|\nabla g| \leq K$, the change is applied.
At first the distribution is calculated for a specific value of $\mathbf{H}_a$ or a specific current I. As $\hat{\mathbf{H}}_a$ and $\hat{\mathbf{I}}$ are zero for the first step $\delta\mathbf{H}_a = \mathbf{H}_a$ and $\delta\mathbf{I} = \mathbf{I}$.
Once there is no change in g that decreases F', the external conditions are modified and $\delta\mathbf{H}_a$ or $\delta\mathbf{I}$ calculated. Once $\delta\mathbf{H}_a$ and $\delta\mathbf{I}$ are found, the process restarts until again finding the g(x,y) distribution minimizing the energyfunction. This step is repeated until the desired external field or external current is reached.
The sheet current $\mathbf{K}(x, y)$, the magnetic induction and the magnetic moment can again be calculated from the resulting g(x,y) distribution.

4 Implementation

The algorithm is seperated in 3 major scripts:

- `getinp.m`
  - input of:
    - the chip dimensions (`dX`,`dY`)
    - the number of gridpoints (`gridpointX` `gridpointY`)
    - a mask to denote the chip geoemtry (`geometrymask`)
    - the boundary conditions (`Ha` and `whole_current`)
  - analysis of the chip geometry:
    - the function `currents.m` searches for chip borders and outputs `general_currentmask`
    - the function `holefinder` looks for connected holeregions and outputs `holemask`
  - initialzation of `coord` for indexing and `neighbourmask`
  - calculation of `Nconst` with the function `N.m`
- `iterate_G.m`
  - looping through chip and calculating energy of $\pm$`dG` in `G` via `energyfunction.m`
  - save energy of variations in `E_varP` and `E_varN`
  - find minimum of `E_varP` and `E_varN`
- `plotter.m`
  Starts the function `plotterfunction` to plot the following data:
  - evolution of the energy during iteration
  - 2d plot of the currents in the chip
  - 3d plot of the magnetic field in z-direction
  - 2d plot of a cut through the current densities along the y-direction

The structure of the algorithm is denoted in the flow diagram 8 on the following page.
In the following we want to take a look on the concrete implementation of this algorithm. Especially the function to evaluate the energy of the a magnetization matrix g called `energyfunction.m`, will be of greater interest, because it represents the calculation intensive operation of this algorithm.

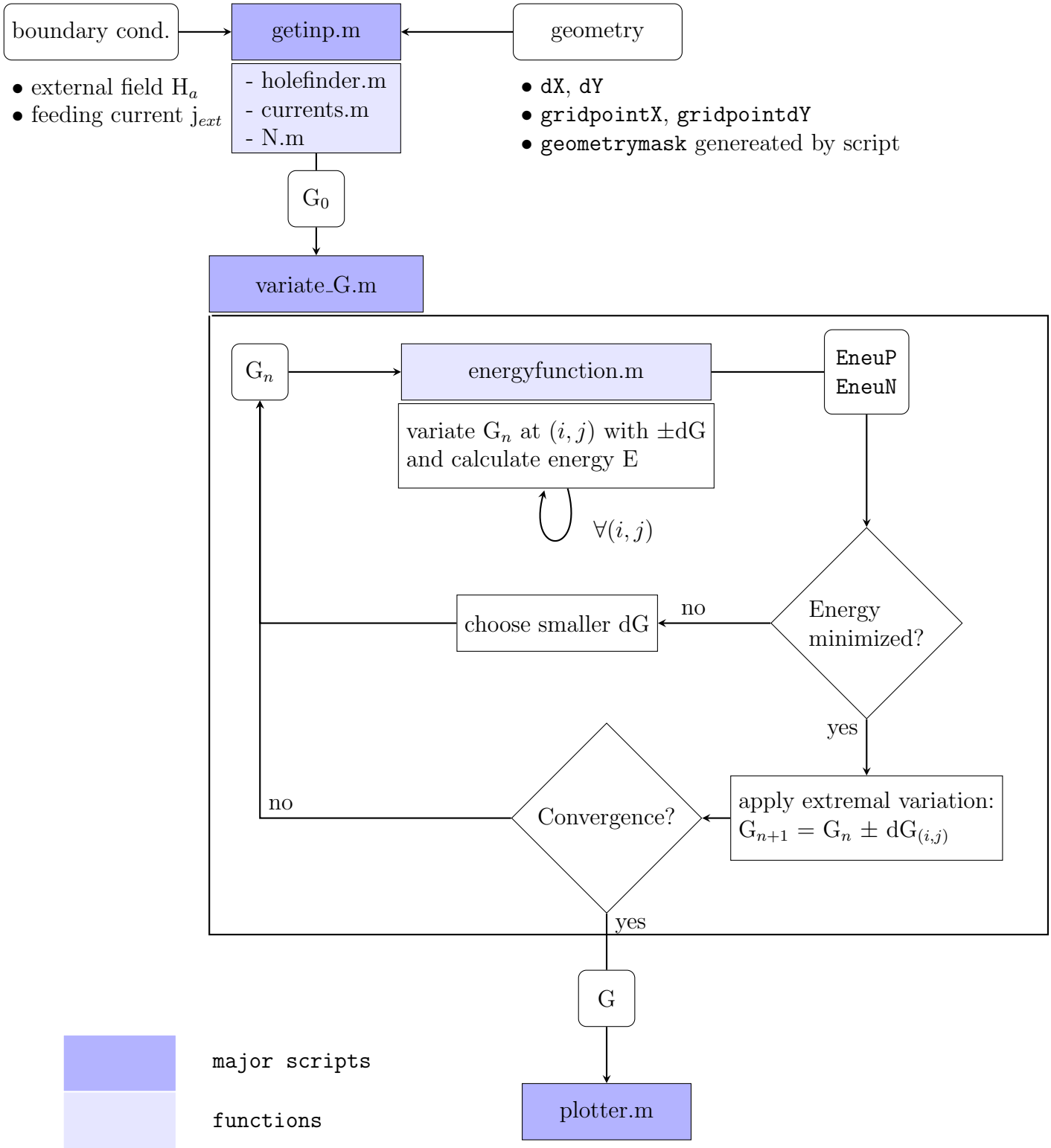

Figure 8: Flowchart of the general structure of the algorithm.

4.1 Geometry

Before the actual algorithm for the calculation of the magnetization matrix g is introduced, a further research of the special geometry of the problem has to be undertaken.
Due to the flat geometry of thin film superconductors used in the experiment (the thickness $t \approx 0.5$nm is in the order of the penetration depth λ), the current distribution along the z-axis can be assumed as constant. Calculations can be restricted to a two dimensional magnetization on the xy-plane, from which the surface-current density $K(x, y)$ can be obtained by equation (15).
Values for the magnetization can be represented as entries in a matrix `G(i,j)` with two spacial indices. The size of this matrix is determined by the number of gridpoints in x and y directions to discretize the chipsource. Without a loss of generality values of g which are located outside the conductor are set to zero.
As proposed by [1] the outer borders of the conducing region can be fixed to zero to simulate absence of external feeding current ($J_{ext} = 0$) and to different values for non vanishing J_{ext}.
Holes inside the chip (isolated regions of insulators totally surrounded by conductor) must have vanishing current. The gradients of the magnetization $g(x, y)$ must vanish due to (15), therefor all entries inside the matrix `G` which coincide with such holes must always have the same value. Variations of the magnetization inside the hole include the variation of all gridpoints which are connected with the insulator region.
The values in `geometrymask` encode regions with different properties:

- **No Conductor**: 0
  On non conducting regions outside the superconductor no variations are applied. All values of the magnetization matrix g in this region are set to zero.

- **Conductor**: 1
  The variation procedure is mainly applied to this values of g. At the beginning of the iteration random noise is added to these values .

- **Borders**: Inf
  The values of g along the borders of the chip are used to implement the boundary conditions and therefor no variation is applied to this region. For an external feeding current I_{ext}, the two border regions are set to $-I_{ext}/2$ on one side and $-I_{ext}/2$ on the other side. For an external magnetic field H_a the magnetization on the borders is set to zero to ensure vanishing net current. The borders of the chip geometry are detected and analyzed by the script `currentfinder`.

Figure 10: Simple strip geometry and the associated matrix `geometrymask`. The numbers denote the cellnumber associated to the gradients calculated by the four values surrounding one cell.

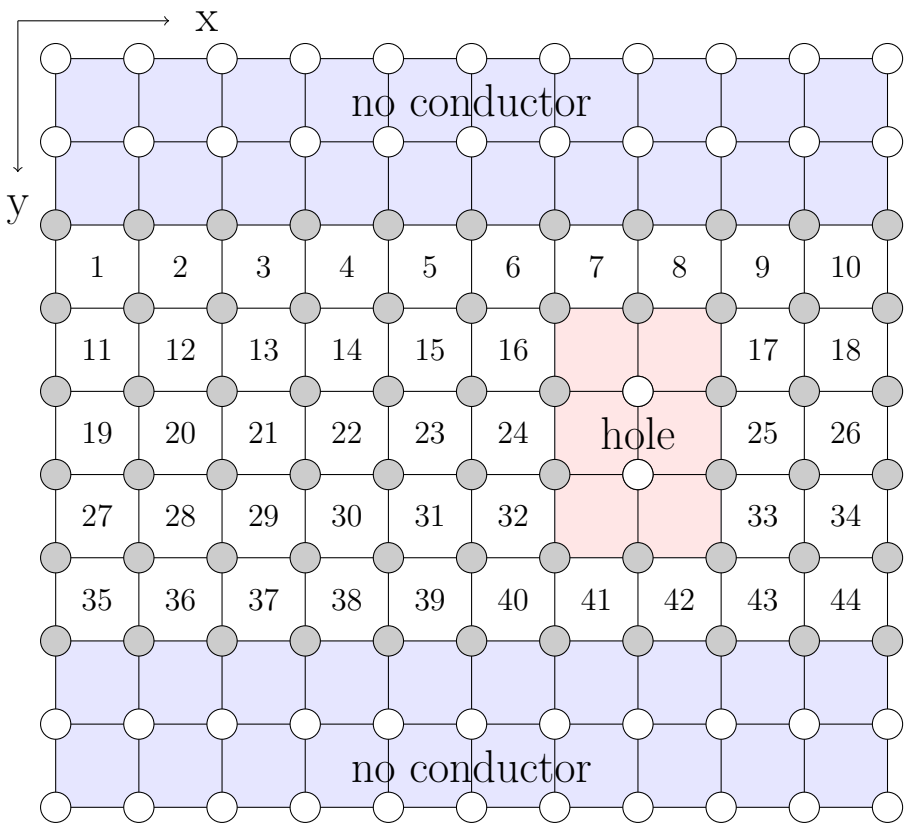

0	0	0	0	0	0	0	0	0	0	0
0	0	0	0	0	0	0	0	0	0	0
Inf	Inf	Inf	Inf	Inf	Inf	Inf	Inf	Inf	Inf	Inf
1	1	1	1	1	1	1	1	1	1	1
1	1	1	1	1	1	1	-1	1	1	1
1	1	1	1	1	1	1	-1	1	1	1
1	1	1	1	1	1	1	1	1	1	1
Inf	Inf	Inf	Inf	Inf	Inf	Inf	Inf	Inf	Inf	Inf
0	0	0	0	0	0	0	0	0	0	0
0	0	0	0	0	0	0	0	0	0	0

- **Holes**: -1, -2, -3, ...
  Connected regions of insulator totally surrounded by conductor must have a vanishing current. Therefor the gradients inside a hole must vanish, that means the values of the magnetization g inside a whole must always be constant. Holes are detected and analyzed by the function `holefinder` and separated holes are noted by negative integers.

Further geometries investigated in this work include a $\frac{\pi}{2}$-turn, an isolated piece of superconductor and the strip with holes.

4.1.1 Indexation

For the implementation of the algorithm (especially for code vectorization) it is useful to define a new index k which indexes every cell with a positive integer instead of the plait of spacial indices in x and y direction (i, j). To connect spacial indices (i, j) with the cellindex k and vice versa a `containers.Map` named `coord` is used, which corresponds to the mapping

$$\text{coord}(x) = \begin{cases} k & \text{if } x = (i, j) \\ (i, j) & \text{if } x = k \end{cases}$$

The indexation of the cells of the discretized magnetization matrix `G` with this new index is illustrated in figure 10, the cells are enumerated row wise.

4.1.2 Nconst

The numerical values of the geometrical scaling factor for the calculation of the self energy of the current $N_{k,k'}$ is shown in 11 for a simple strip geometry (10×10 gripoints). The time intensive evaluation is implemented by the scripts `N` and `T` and is performed a single time within the script `getinp`.

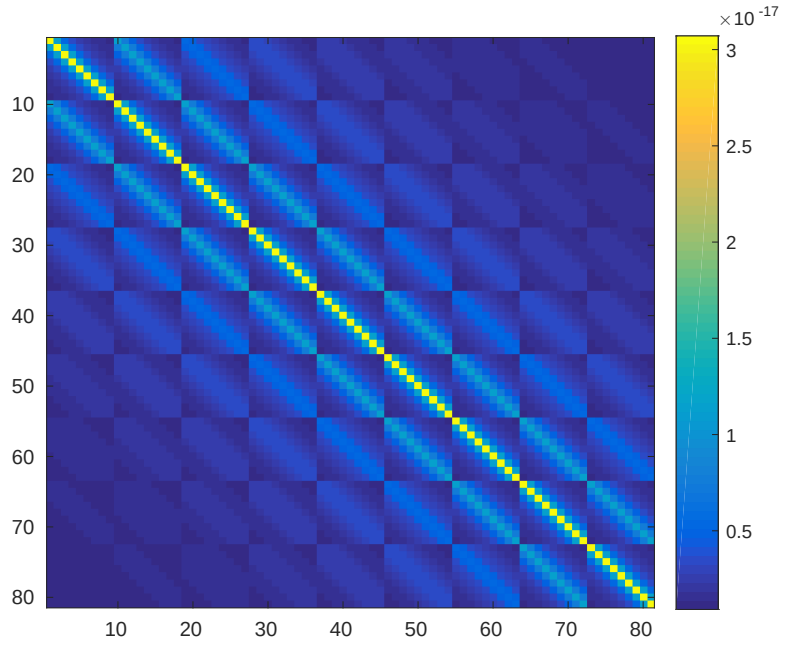

Figure 11: Values of the matrix `Nconst`, discretized approximation for the integral $N_{k,k'}$.

4.2 Energy calculation

The energy has to be calculated at every iteration step for any entry in g with a positive and negative variation Δg, that means for n gridpoints the energy of the magnetisation has to be calculated $2n$ times. Therefor optimaziation of the energy-functional will reduce computation time significantly.
Several versions of `energyfunction` were developed and tested which shall be discussed in the following section. For the calculation of the results presented in the next section the delta-energy method was used.

4.2.1 First energyfunction

The first attempt to implement the energyfunction uses `for` loops:

- over the two spacial indices $(i, j) \in \{1, ..., \texttt{gridpointX}\} \times \{1, ..., \texttt{gridpointY}\}$
- and the cellindex $k \in \{1, ..., \texttt{cellnumber}\}$ with $\texttt{cellnumber} \propto \texttt{gridpointX} \cdot \texttt{gridpointY}$

The three quantities `Eint`, `Eext` and `Ekin` which sum up to the total energy of the magnetization g are calculated by summations as proposed by equation 25–27.

The function `energyfunction.m` to calculate the total energy has the following structure:

```
function [E] = energyfunction(G,Ha,Nconst,Lambda,geometry)

%% Computation of gradient matrices in x and y direction
gradGY = zeros(gridpointX,gridpointY-1);
gradGX = zeros(gridpointX-1,gridpointY);

for i = 1:gridpointY-1
    for j = 1:gridpointX-1
        gradGY(i,j) = 0.5 * deltaY * (G(i+1,j)-G(i,j)+G(i+1,j+1)-G(i,j+1));
        gradGX(i,j) = 0.5 * deltaY * (G(i,j+1)-G(i,j)+G(i+1,j+1)-G(i+1,j));
    end
end

%% 1) Compuatuion of Eint
%%folding integral over grad(G) with cellindex k
Eint = 0;
for k1 = 1:real_cellnumber
    for k2 = 1:real_cellnumber
        Eint = Eint + 0.5 * my ...
            * (gradGY(k1)*gradGY(k2) + gradGX(k1)*gradGX(k2))...
            * Nconst(k1,k2);
    end
end

%% 2) Computation of Eext
%%average of each cell with spacial indices (i,j)
Eext = 0;
for i = 1:gridpointY-1
    for j = 1:gridpointX-1
        Eext = Eext + 0.25 * my * Ha * (deltaX*deltaY) ...
            * (G(i,j)+G(i+1,j)+G(i,j+1)+G(i+1,j+1));
    end
end

%% 3) Computation of Ekin
%%absolute value of grad(G)
Ekin = 0;
for k = 1:real_cellnumber
    Ekin = Ekin + 0.5 * my * Lambda * (deltaX*deltaY) ...
```

```
40      * (gradGX(k)*gradGY(k)+gradGX(k)*gradGX(k));
41  end
42
43  %% Total energy E
44  E = Eext + Ekin + Eint;
45
46  end
```

By the structure of the code the computational effort can be analyzed depending on the number of gridpoints used to discretize the chip:

1. `Eint`

   The first summation for the folding integral of `Eint` goes over two cellindices (k_1,k_2). k is proportional to (`gridpointX` · `gridpointY`), that means the summation with $(k1, k2)$ is proportional to $(\texttt{gridpointX} \cdot \texttt{gridpointY})^2$.

   The result of this folding of G_x and G_y is then multiplied with `Nconst`, the discretized value of the folding integral $N_{k,k'}$.

2. The other two summations for `Eext` and `Ekin` are proportional to $(gridpointX \times gridpointY)$, the computational effort is proportional to the number of cells used to discretize the chip.

Intensive testing with this algorithm has shown that the biggest part of the calculation time is consumed by the calculation of `Eint`.

4.2.2 Vectorized energyfunction

This vectorized energyfunction uses optimized matrix algebra to circumvent performance weaknesses of looping through the chip.
Arranging the gradients G_x and G_y in vectors with the length `cellnumber`, gives the possibility to calculate the internal energy E_{int} with the operation

$$E_{int,array} = \frac{\mu}{2} \cdot (G_x \otimes G_x + G_y \otimes G_y) \cdot N_{k,k'} \tag{33}$$

and the following summation of the generated matrix $E_{int,array}$. Also the calculation of E_{ext} and E_{kin} has been rewritten using matrix algebra and summation of the generated energy matrices.

```
1  function [E] = energyfunction(G,Ha,Nconst,Lambda,geometry)
2
3  %%...
```

```
%%... generation of gradient vectors gradGY_vec, gradGX_vec from G
%%...

%% 1) Compuatuion of Eint
Eint_array = (gradGY_vec*gradGY_vec'+gradGX_vec*gradGX_vec').*Nconst;
Eint = 0.5 * my * sum(sum(Eint_array));

%% 2) Computation of Eext
Eext_array = G1 + G2 + G3 + G4;
Eext = 0.25 * my * Ha * (deltaX*deltaY) * sum(sum(Eext_array));

%% 3) Computation of Ekin
Ekin_array = gradGX.*gradGX + gradGY.*gradGY;
Ekin = 0.5 * my * Lambda * (deltaX*deltaY) * sum(sum(Ekin_array));

%% Total energy E
E = Eext + Ekin + Eint;

end
```

Intensive testing of this rewritten energyfunction and analysis of the run-time show that great part of it is consumed by the summation of the matrix generated by (33) and only a further approach to reduce the number of computations executed will lead to run-times affordable for acceptable resolution.

4.2.3 Delta energyfunction

Due to bad performance with resolutions bigger than 20×20 gridpoints a further investigation to speed up the code was necessary.
The calculation time can be reduced significantly by introducing a new function which calculates only the energies which change by a variation of a single value of the magnetization. Within the double-sum for the self-interaction of the currents

$$E_{int} = \frac{\mu}{2} \cdot \sum_{k} \sum_{k'} G_{x,k} \cdot G_{x,k'} + G_{y,k} \cdot G_{y,k'} \tag{34}$$

most of the values stay the same after a variation of g at a specified coordinate (i, j). As illustrated in 12 a change of the magnetization ΔG alters the values for the gradients defined inside adjacent cells k_1, k_2, k_3 and k_4. Therefor only four rows and columns inside the matrix with the energy of self interaction change their values, which can be seen by decomposing the matrix product in 34 with the upper four indices of k (G^o represent the values of the magnetisation gradients before a variation, G^n are the gradients with one value changed, for better readability the distinction between gradients in x and y direction is surpressed):

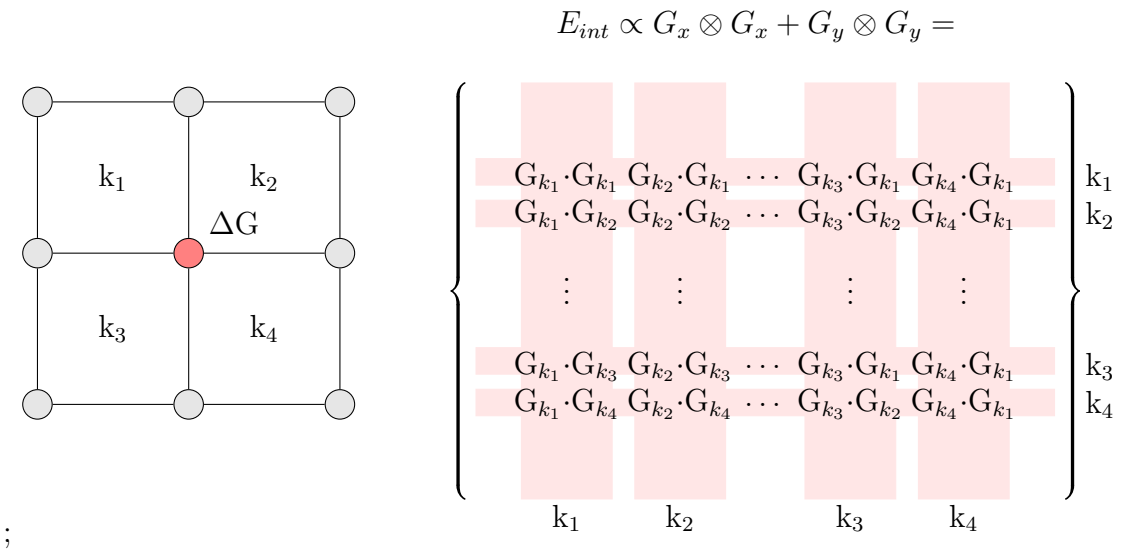

;

Figure 12: A change ΔG of a single value of the magnetization, has only effect on four rows and four columns in the matrix for the self-interaction of the currents.

$$
\begin{aligned}
\Delta E_{int} &= E_{int}^{new} - E_{int}^{old} \qquad (35)\\
&\propto \sum_{k,k'} G_k^n \cdot G_{k'}^n - G_k^o \cdot G_{k'}^o \\
&\propto 2\sum_{k'} [G_{k1}^n + G_{k2}^n + G_{k3}^n + G_{k4}^n]G_{k'}^n - [G_{k1}^o + G_{k2}^o + G_{k3}^o + G_{k4}^o]G_{k'}^o \\
&\quad -G_{k1}^n G_{k1}^n - G_{k1}^n G_{k2}^n - ... - G_{k4}^n G_{k3}^n - G_{k4}^n G_{k4}^n \\
&\quad +G_{k1}^o G_{k1}^o + G_{k1}^o G_{k2}^o + ... + G_{k4}^o G_{k3}^o + G_{k4}^o G_{k4}^o \\
&\quad + \underbrace{\sum_{\substack{k\neq k1,k2,k3,k4 \\ k'\neq k1,k2,k3,k4}} G_k^n \cdot G_{k'}^n - G_k^o \cdot G_{k'}^o}_{=\ 0,\ \text{because } G^n = G^o \text{ for these indices}}
\end{aligned}
$$

The last term with the double-sum in equation 36 vanishes, because the values for the gradients of the magnetisation have not changed. The first term represents a sum over the index $k \in \{1, ..., \texttt{cellnumber}\}$, the third and fourth line represent correction terms which are counted double by the previous line. Therefor the computational effort to calculate E_{int} can be reduced from $\mathcal{O}(n^2)$ to $\mathcal{O}(n)$ with the number of gridpoints n.
This procedure is implemented by the function `delta_energyfunction`, which calculates the change of self-interaction energy by summing the four rows and

columns with changing values and subtracting double counting of the indices where rows and columns cross each other within the self-interaction matrix.
For the interaction energy with the external field E_{ext} and the kinetic energy E_{kin} a similar approach has been implemented, despite of the fact that the calculation of those energies has a negligible contribution to the computation time.

4.2.4 Performance analysis

By calculating the differences in the energies a distinctive speedup of the alculation time could be approached. Calculations were performed on grids with up to 2500 points. The difference in the calculation time for one evaluation of the energy functional with and without the energy difference method is shown in figure 13.

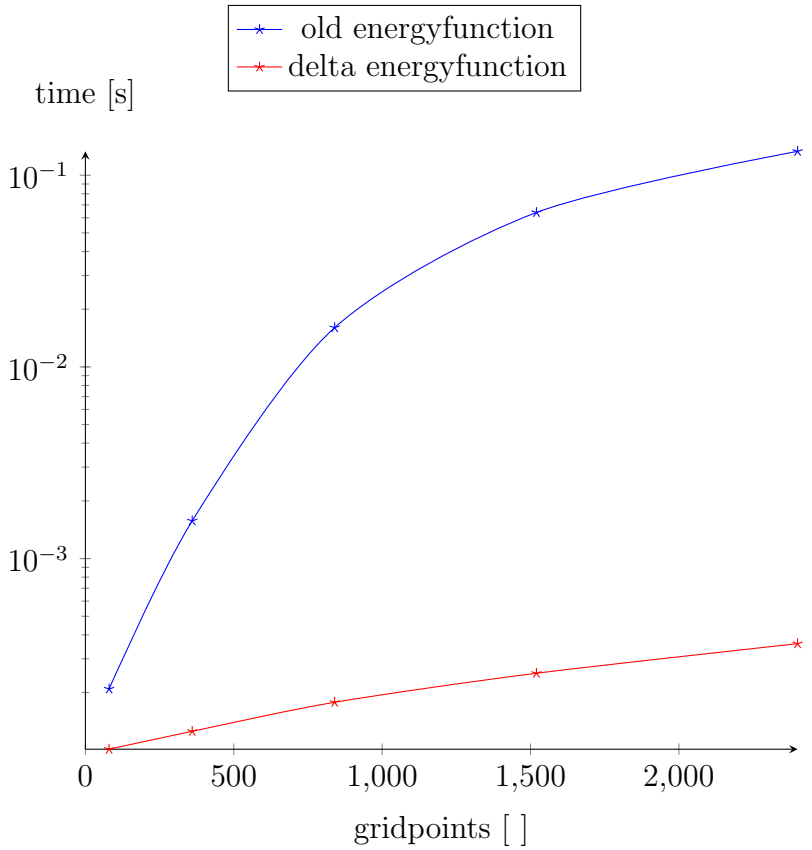

Figure 13: Comparison of the average computation time of one energy calculation with the old energyfunction and the delta method.

5 Results

5.1 Meissner state

The Meissner state has been simulated for four different geometries: the generic strip, the $\frac{\pi}{2}$-turn, the strip with a hole and an isolated piece of conductor. Simulations were performed on grids with 50×50 gridpoints, the width of the conducting track is W = 10μm corresponding to the dimensions of the atom-chips used in the experiment. The London penetration depth for the yttrium-barium-copper-oxide (YBCO) is assumed as $\lambda_L = 35{\cdot}10^{-9}$m. Therefor the ratio $\frac{\Lambda}{W} \approx 1$, which means that the solutions will be somewhere between the 'complete shielding' ($\frac{\Lambda}{W} \ll 1$) where only a thin layer of shielding current flows along the surface and the 'narrow' case ($\frac{\Lambda}{W} \gg 1$) where the hole conductor is penetrated by the currents (see [1]).
For the chosen resolutions calculations were performed until no significant change of the magnetic energy of the system was noticed, which happened between 30000 and 60000 iteration steps (≈ 5-10 hours run-time).
In the following section we want to take a closer look at the concrete results and compare them to the outcomes of [1].

5.1.1 Strip

The straight strip is the most simple geometry for a superconducting chip. Analytic solutions for the strip are given by [1], so the strip can be used to verify the correctness of the algorithm.
The first simulation performed was the straight strip with only an external current I_a applied, shown in figure 14). As expected, applying a current along the x-axis lead to an exponential decay of the current density towards the center of the superconductor. The current is squeezed to a thin layer of shielding currents of the magnitude of λ.
These shielding currents shown in image (a) result in (b), where a strong located magnetic field can be seen along the borders of the strip due to the higher current density. As expected, applying higher currents provoke higher current densities at the borders of the strip, as illustrated in image (c). Note that image (c) is only representative for the currents in the x-direction K_x along the y-axis for one specific value of x = 1μm of the strip. In (d) a cut through the magnetic induction in z-direction (at z = 0) can be seen, which shows the typical sharp minimum and maximum of the field at the borders. The biggest part of the superconductor is nearly field free as expected.
In figure 15 resulting currents ((a) and (c)) and magnetic induction ((b) and (d)) are shown for an applied external field H_a. As $I_a = 0$ the net current must be zero, which is attained by two currents with opposite directions. Again currents

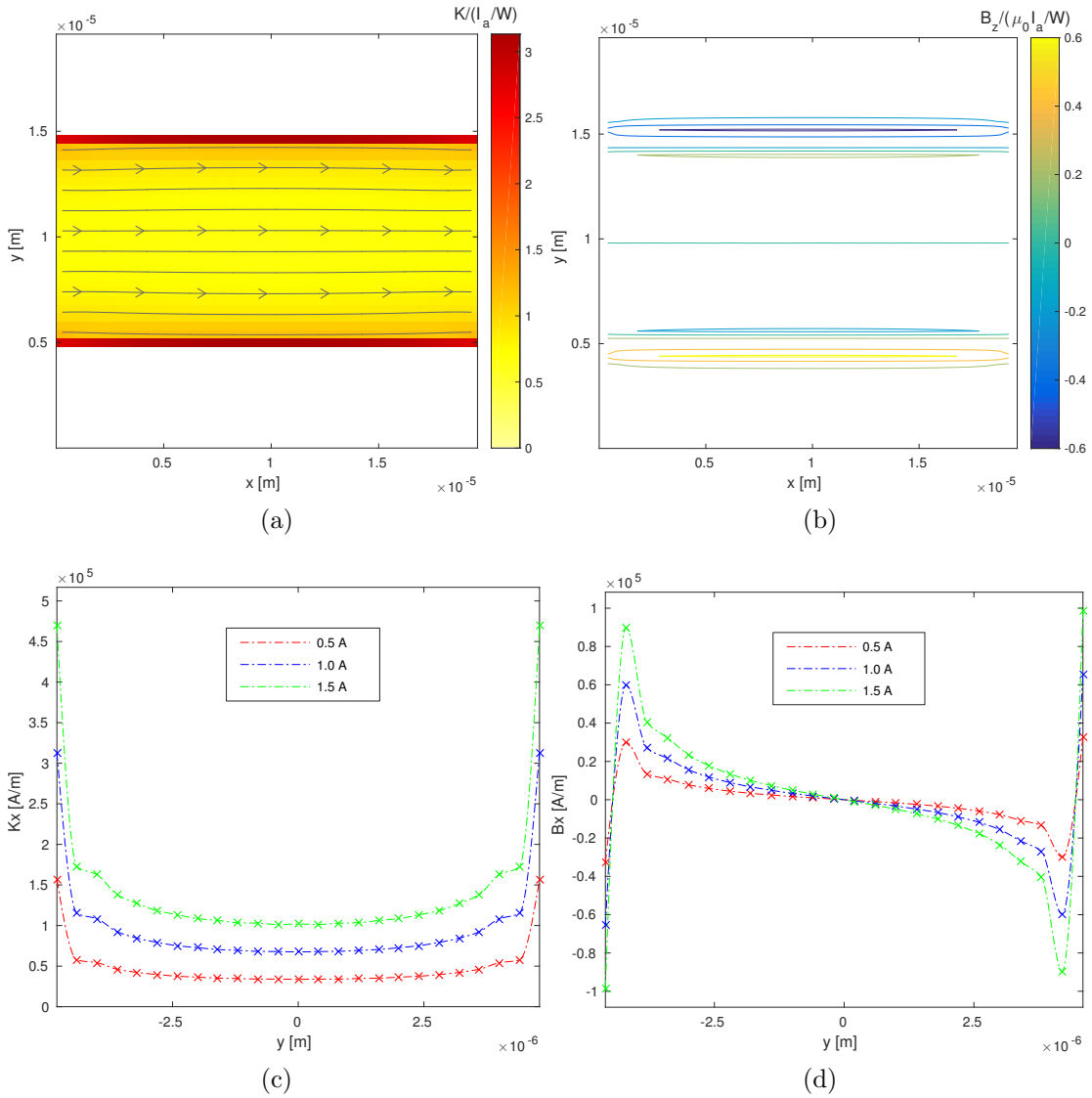

Figure 14: Simulation of a straight strip with external current I_a applied. (a) Current stream lines for $I_a = 1.5$A and (b) magnetic induction for $I_a = 1.5$ A. Below: Cut through the straight strip at x = 1μm for different currents applied. red line: $I_a = 0.5$A, blue line: $I_a = 1.0$A, green line: $I_a = 1.5$A (c) resulting current stream lines (d) resulting magnetic field lines

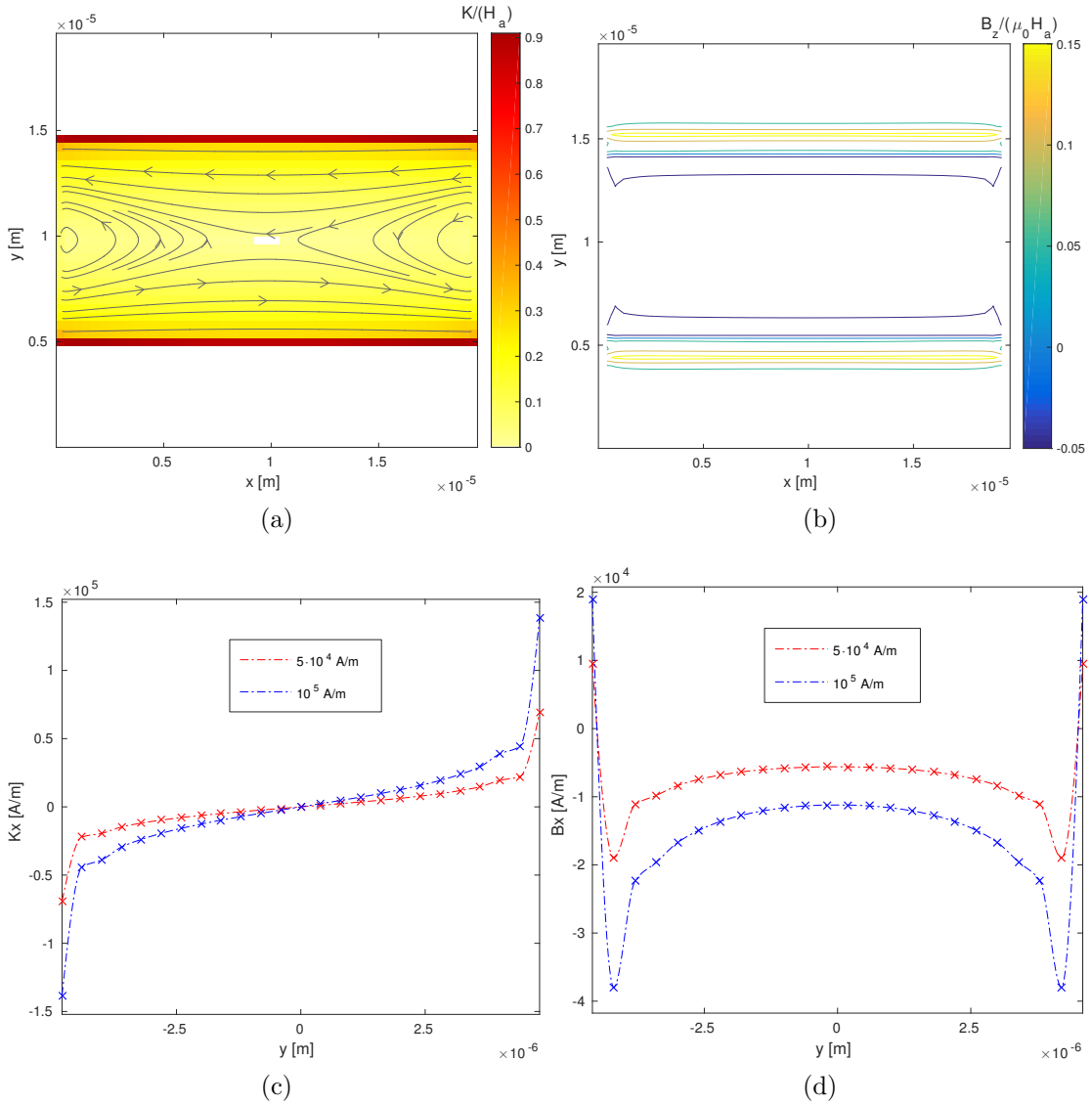

Figure 15: Simulation of a straight strip with external magnetic field H_a applied. (a) Current stream lines and (b) magnetic induction for $H_a = 10^5$ A/m. Below: cut through the straight strip at x = 1μm for different fields. red line: $H_a = 5{\cdot}10^4$ A/m, blue line: $H_a = 10^5$ A/m (c) resulting current stream lines (d) resulting magnetic field lines

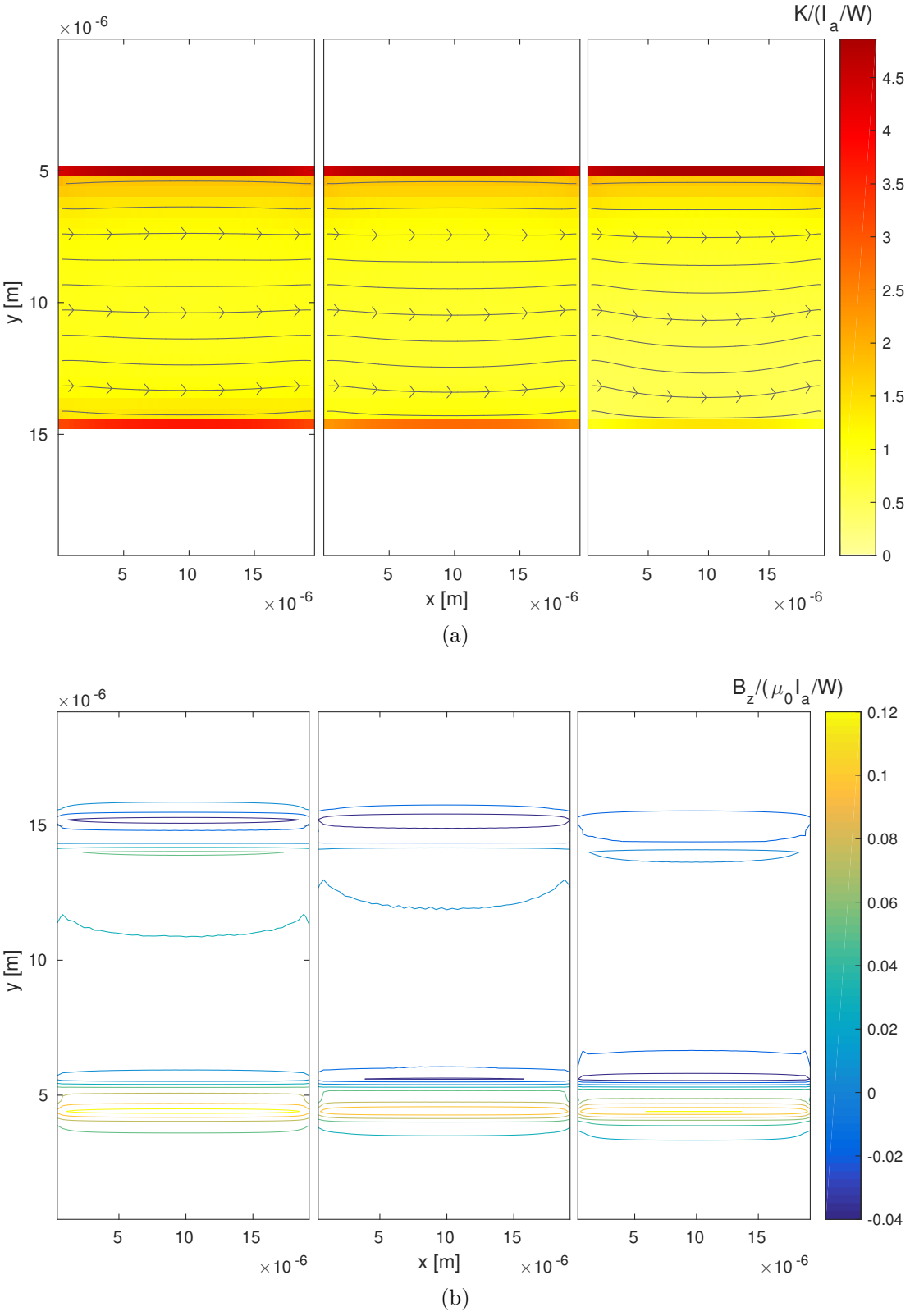

Figure 16: Simulation of a straight strip with external magnetic field H_a and feeding current I_a applied. (a) Current stream lines and (b) magnetic induction for $I_a = 1$A and different fields $H_a = 5{\cdot}10^4$ A/m, 10^5 A/m and $2{\cdot}10^5$ A/m.

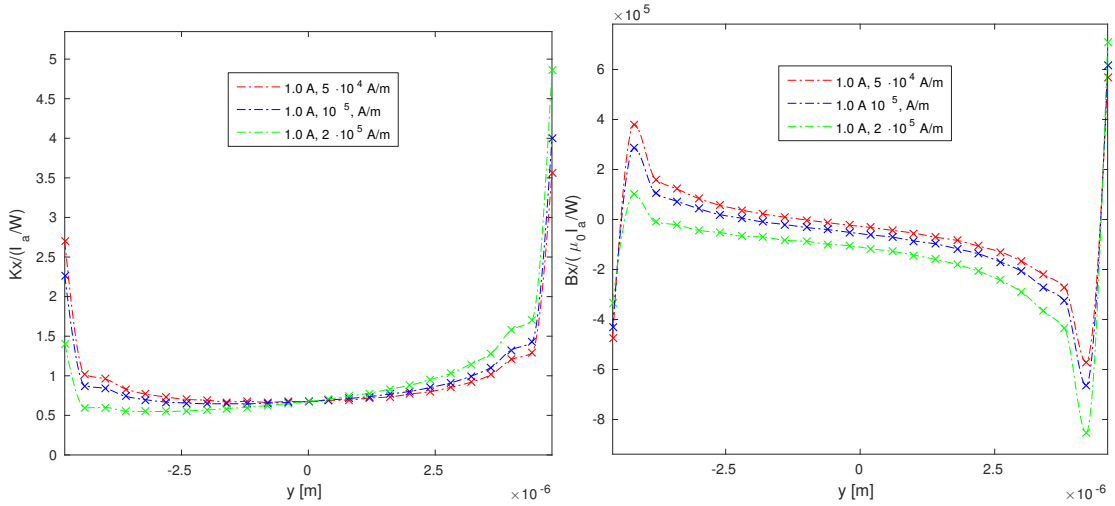

(a) (b)

Figure 17: Cut through the straight strip at x = 1μm for different fields and the current I_a = 1 A. red line: $H_a = 5{\cdot}10^4$ A/m, blue line: $H_a = 10^5$ A/m, green line: $2{\cdot}10^5$ A/m. (a) resulting current stream lines (b) resulting magnetic field lines

are squeezed to the borders, the inner part of the conductor is nearly current free. The magnetic induction produced by the currents is symmetric to the y-axis, with sharp minima inside the conductor near the border, and maxima exactly at the border.
In figure 16 and 17 a current of I_a = 1A is applied together with external field H_a ranging from $5{\cdot}10^4$ A/m to $2{\cdot}10^5$ A/m. From the current densities the effect of the superposition with the field can be seen: the field lowers the current density at one border and enlarges it on the other side. The field can be chosen big enough to annihilate the current squeezing at one border. Current and generated magnetic induction are asymmetric in reference to the strip applied only to external fields or only to an external feeding current. This behaviour matches with the predictions given by [1].

5.1.2 Strip with a $\frac{\pi}{2}$-turn

The $\frac{\pi}{2}$-turn is a geometry present in the Z geometry, which is used by the experiment. Again the conducting track has a width of W = 10 μm.
For the transport current case (figure 18) there is a similar behaviour to the strip: the current is squeezed to the borders, maxima and minima of the magnetic induction appear along borders. In addition to that behaviour the special geometry has a major influence on the current distribution: near the corner at (x,y) =

(1μm,1μm) the current is crowding and produces a localized maximum of the magnetic induction. The current density at the outer corner of the turn is decreasing respectively. As mentioned by [1] that is a pure geometrical effect which also happens in conventional conductors due to turns or widenings.
Also in the case of an external field (figure 19) the influence of the $\frac{\pi}{2}$-turn can be seen. Again there are two counter-wise oriented currents, giving zero net-current. In addition to the increase/decrease of the current density at the inner/outer corner of the turn, current circulations arise at the middle of the corner.
The cuts through current and induction in figure 18 and 19 ((c) and (d)) show a slight asymmetry depending on the distance to the corner, which is most prominent at the inner border near the corner.

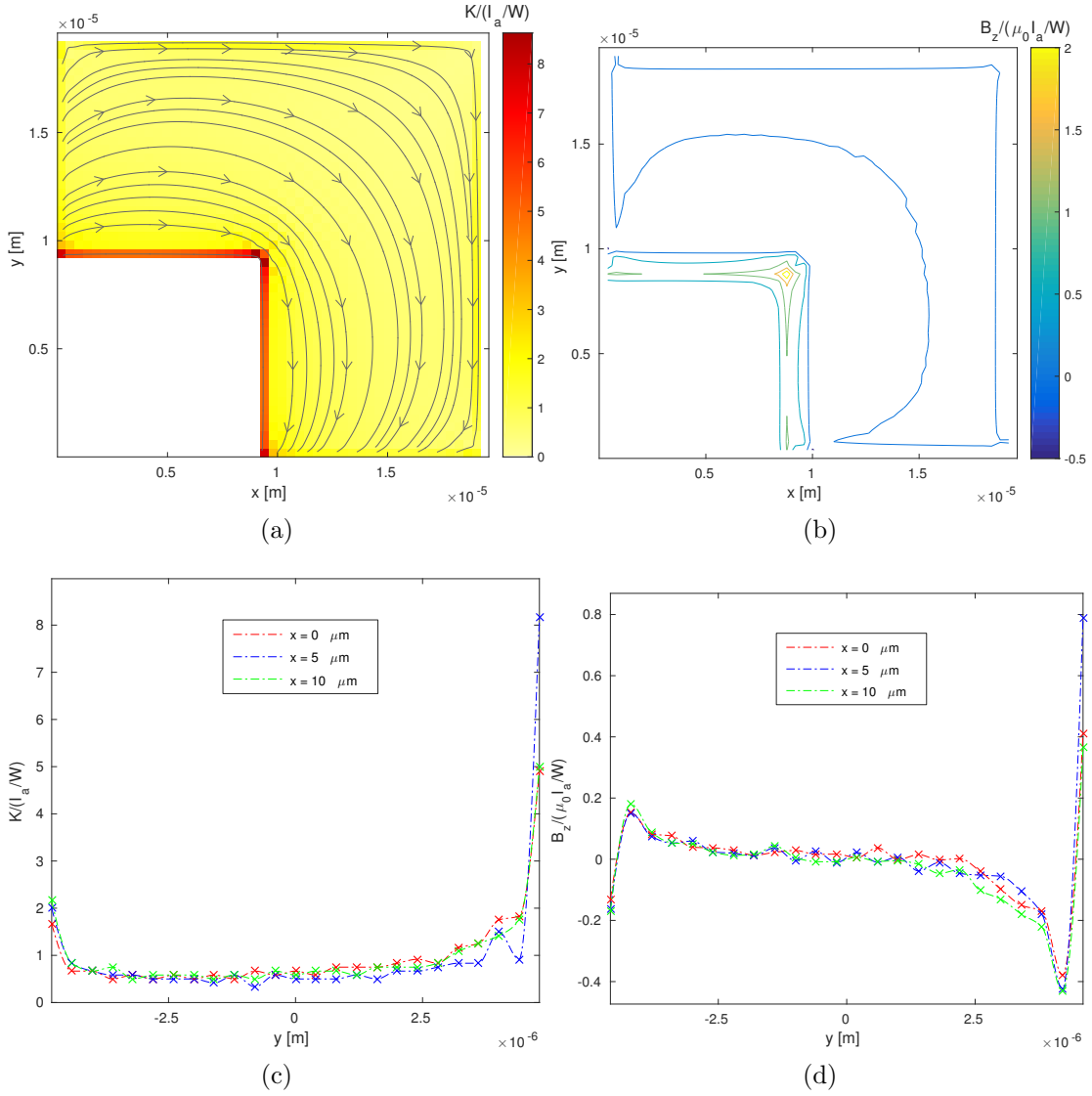

Figure 18: Simulation of a strip with a $\frac{\pi}{2}$-turn with external current I_a applied. (a) Current stream lines and (b) magnetic induction for $I_a = 1.5$A. Below: cut through the strip at x = 0μm (red line), x = 5μm (blue line) and x = 10μm (green line) with (c) resulting current stream lines and (d) resulting magnetic induction.

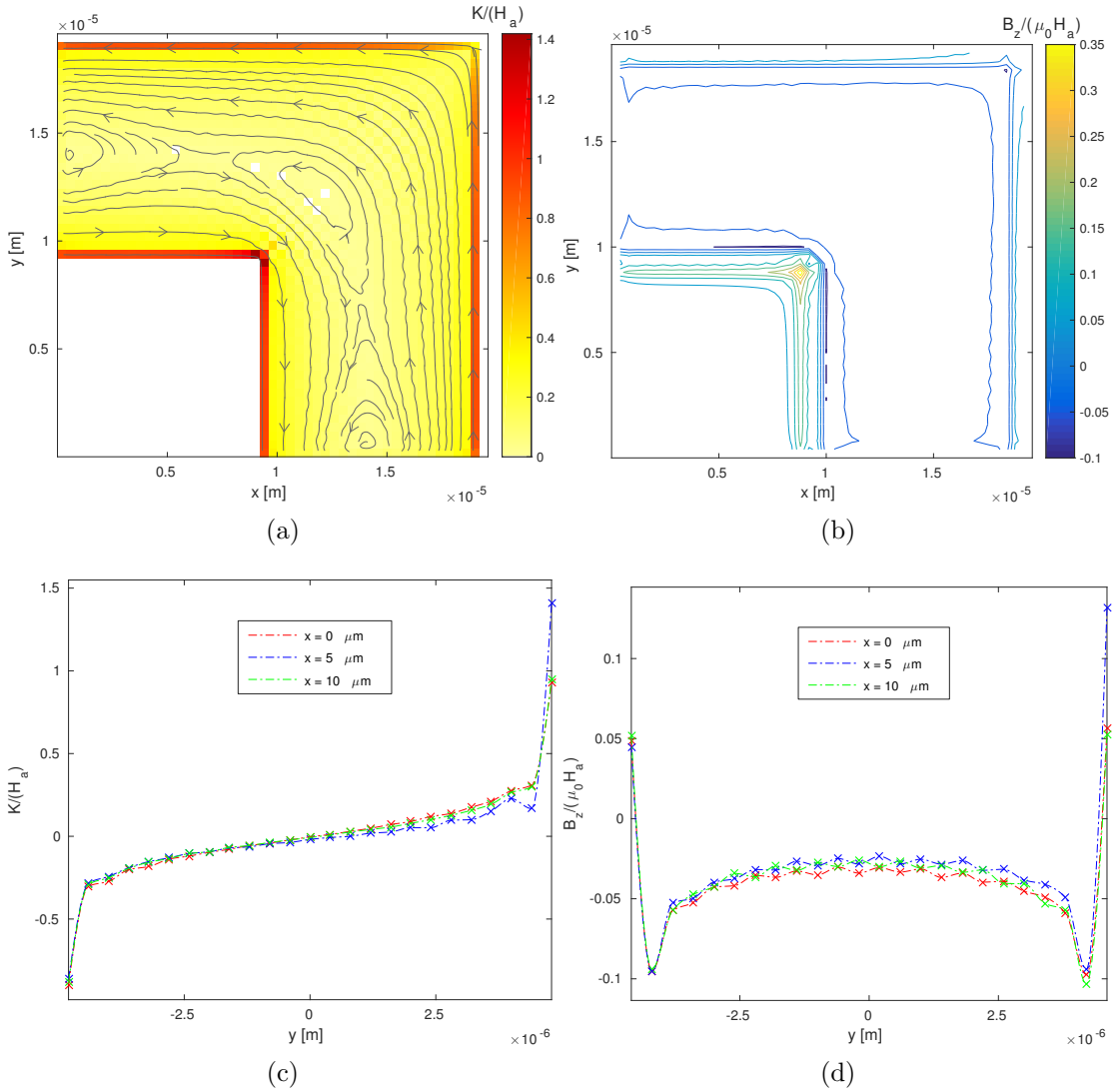

Figure 19: Simulation of a strip with a $\frac{\pi}{2}$-turn with external field H_a applied. (a) Current stream lines and (b) magnetic induction for $H_a = 10^5 A/m$. Below: cut through the strip at $x = 0\mu m$ (red line), $x = 5\mu m$ (blue line) and $x = 10\mu m$ (green line) with (c) resulting current stream lines and (d) resulting magnetic induction.

5.1.3 Strip with a hole

Calculations were also performed on the strip with a hole of size $W/3 = 0.33 \cdot 10^{-5}$m. For the case of external feeding current an increase of the current density near the hole has been observed (figure 20). That is due to the classical effect of current crowding at narrowings which the hole imposes on the strip.
Also the case of an applied external field has been studied (figure 21). The current crowding has not been observed because the currents to the left and right of the hole change their direction before they can lap over the defect the hole represents.

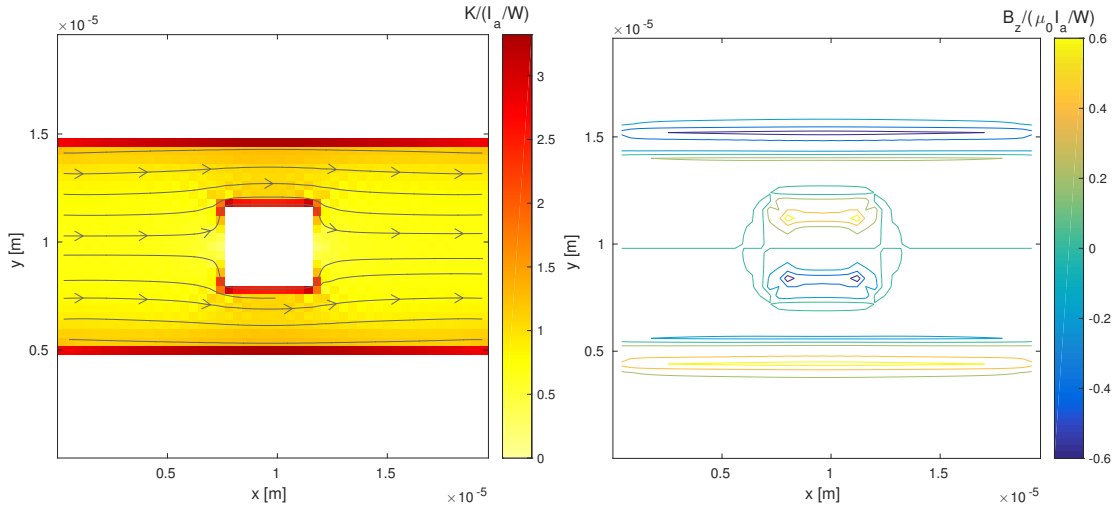

Figure 20: Simulation of a strip with a hole of size $W/3 = 0.33 \cdot 10^{-5}$m with external current $I_a = 1.0$A applied. (a) resulting current stream lines and (b) magnetic induction.

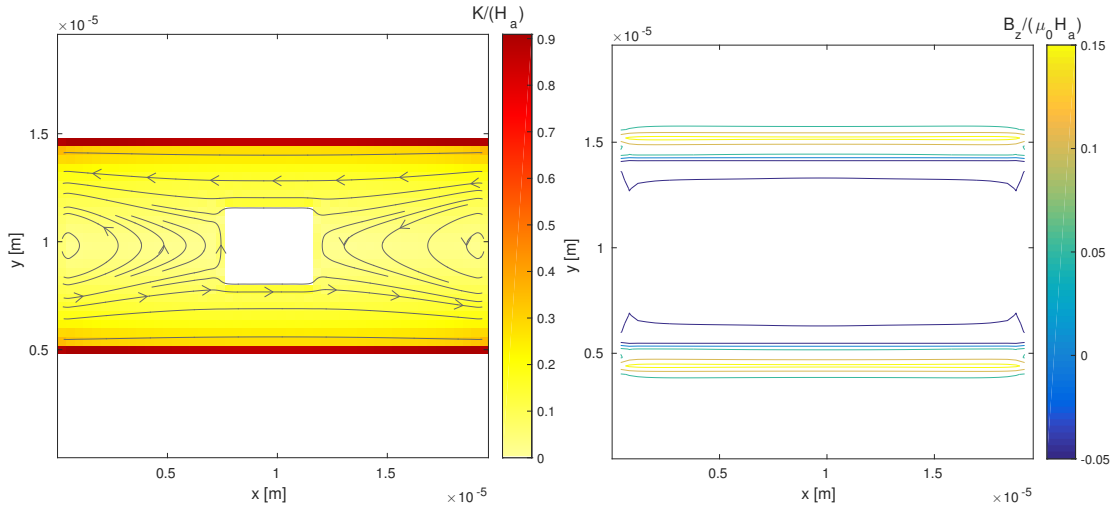

(a) (b)

Figure 21: Simulation of a strip with a hole of size $W/3 = 0.33 \cdot 10^{-5}$m with external field $H_a = 10^5$A/m applied. (a) resulting current stream lines and (b) magnetic induction.

5.1.4 Island

Calculations were performed on an isolated square of conductor with an edge length of $W = 10$ μm. Due to the missing connection to feeding wires only an applied field was tested with this geometry. The current inside the superconductor arranges itself to a circular flow which generates a field minimum at the center of the conductor and elongated maxima along the borders.

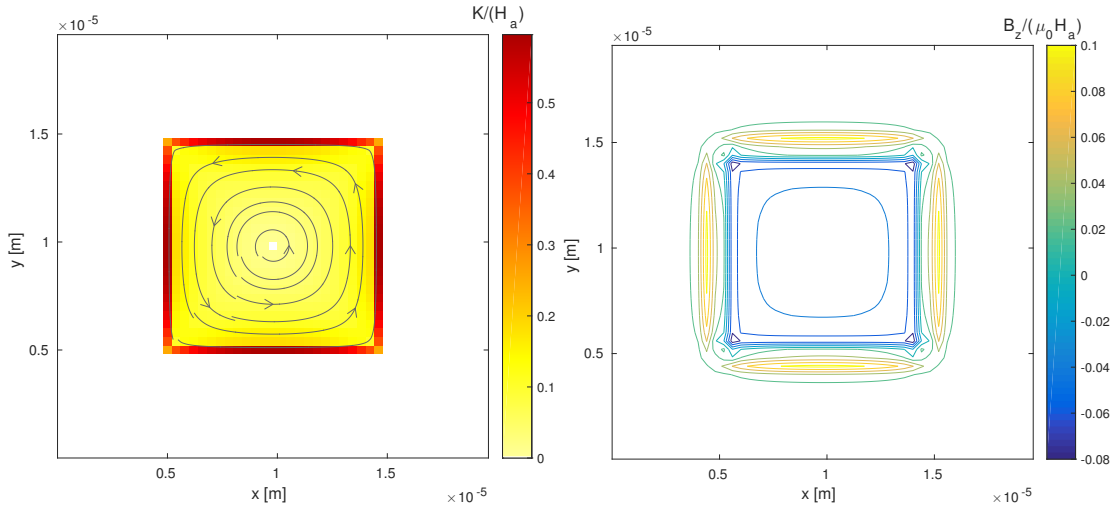

(a) (b)

Figure 22: Simulation of an isolated piece of conductor subjected to an external magnetic $H_a = 10^5 A/m$. (a) resulting current stream lines and (b) magnetic induction.

References

[1] C. Navau A. Sanchez, G. Via. *Magnetic and transport currents in thin film superconductors of arbitrary shape within the london approximation.* Journal of Applied Physics, 113, 2014.

[2] C. Navau-N. Del-Valle A. Sanchez, G. Via. *Simultaneous magnetic and transport currents in thin film superconductors within the critical-state approximation.* Superconductor Science and Technology, 28, 2014.

[3] E.H. Brandt. *Thin superconductors and SQUIDs in perpendicular magnetic field.* Physical Review B 72, 024529, 2005.

[4] N. Del-Valle D.-X. Chen C. Navau, A. Sanchez. *Alternating current susceptibility calculations for thin-film superconductors with regions of different critical-current densities.* Journal of Applied Physics 103, 113907, 2008.

[5] A.P. Malozemoff C.M. Rey. *Superconductors in the Power Grid.* Woodhead Publishing Series in Energy, 2015.

[6] R. Flükiger. *Overview of Superconductivity and Challenges in Applications.* Reviews of Accelerator Science and Technology, 2012.

[7] M. Reissner S. Bühler-Paschen, H. Michor. *Festkörperphysik I.* E138-Institut für Festkörperphysik, 2015.

[8] R. Kleiner W. Buckel. *Supraleitung: Grundlagen und Anwendungen.* Wiley-VCH, 2013.

6 Appendix

Numerical approximation for $N_{k,k'}$

$$
\begin{aligned}
N_{kk'} = & T(x_{k'} + \Delta X_{k'}, x_k + \Delta X_k, y_{k'} + \Delta Y_{k'}, y_k + \Delta Y_k) \\
& - T(x_{k'} + \Delta X_{k'}, x_k + \Delta X_k, y_{k'} + \Delta Y k', y_k) \\
& - T(x_{k'} + \Delta X_{k'}, x_k, y_{k'} + \Delta Y_{k'}, y_k + \Delta Y_k) \\
& + T(x_{k'} + \Delta X_{k'}, x_k, y_{k'} + \Delta Y_{k'}, y_k) \\
& - T(x_{k'}, x_k + \Delta X_k, y_{k'} + \Delta Y_{k'}, y_k + \Delta Y_k) \\
& + T(x_{k'}, x_k + \Delta X_k, y k' + \Delta Y_{k'}, y_k) \\
& + T(x_{k'}, x_k, y_{k'} + \Delta Y_{k'}, y_k + \Delta Y_k) \\
& - T(x_{k'}, x_k, y_{k'} + \Delta Y_{k'}, y_k) \\
& - T(x_{k'} + \Delta X_{k'}, x_k + \Delta X_k, y_{k'}, y_k + \Delta Y_k) \\
& + T(x_{k'} + \Delta X_{k'}, x_k + \Delta X_k, y_{k'}, y_k) \\
& + T(x_{k'} + \Delta X_{k'}, x_k, y_{k'}, y_k + \Delta Y_k) \\
& - T(x_{k'} + \Delta x_{k'}, x_k, y_{k'}, y_k) \\
& + T(x_{k'}, x_k + \Delta X_k, y_{k'}, y_k + \Delta Y_k) \\
& - T(x_{k'}, x_k + \Delta X_k, y_{k'}, y_k) \\
& - T(x_{k'}, x_k, y_{k'}, y_k + \Delta Y_k) \\
& + T(x_{k'}, x_k, y_{k'}, y_k)
\end{aligned}
$$

with T(x,x',y,y') being

$$
\begin{aligned}
T(x, x', y, y') = & -\frac{1}{6}[(x - x')^2 + (y - y')^2]^{3/2} \\
& + \frac{1}{2}(x - x')(y - y')\Big\{ \ (y - y')log\Big[\ x - x' + \sqrt{(x - x')^2 + (y - y')^2}\Big] \\
& + (x - x')log\Big[\ y - y' + \sqrt{(x - x')^2 + (y - y')^2}\Big] \ \Big\}
\end{aligned}
$$

Variables defined by the algorithm

The major arrays of the algorithm (n and m are the number of gridpoints in x and y direction, l is the number of conducting cells proportional to $(n-1 \times m-1)$ called `realcellnumber` in the code):

variable name	size	description
`G`(i,j)	$(n \times m)$	Magnetisation matrix
`Nconst`(k,k')	$(l \times l)$	Numerical solution of the double surface integral $N_{k,k'} = \frac{1}{4\pi} \int\int \frac{1}{\sqrt{(x-x')^2+(y-y')^2}} dS dS'$ (aside from rounding mistakes, this tensor is symmetric)
`coord`(k,a)	$(l \times 3)$	Connects a cell index k with its adjacent node coordinates x ($a = 2$) and y ($a = 3$)
`coord_array`(i,j)	$(n-1 \times m-1)$	Connects node coordinates (i, j) wiht the cell index k
`neighbourmask`(a,b,i,j)	$(2 \times 2 \times n-1 \times m-1)$	Contains a 2×2 submatrix for every node (i, j). Its entries are the cellnumber or 0 for missing conductor.
`geometrymask`(i,j)	$(n \times m)$	Is an input mask to define a special geometry on the chip (1 means conductor,

		0 no conductor)
`general_currentmask`(i,j) `currentmask`(i,j)	$(n \times m)$	Implements border regions with external feeding current and their value (`Inf` for no current boundary condition)
`holemask`(i,j)	$(n \times m)$	G sized array which implements holeregions, produced by the function `holefinder.m`
`E_varP` `E_varN`	$(n-1 \times m-1)$	The effect of positive and negative variations on the energy are saved in this arrays

Only the the first two arrays carry the data needed for the calculation, the rest is for indexing in a compact and easy manner.

The structure `geomtry` is a collection of variables defining the geometrical scaling of the above arrays, and the meaning of their elements. It is composed by:

variable name	description
`dX`	dimensions of the chip source [m]
`dY`	
`gridpointX`	number of gridpoints in x and y direction
`gridpointY`	
`deltaX`	dimensions of a single cell [m]
`deltaY`	
`realcellnumber`	number of cunducting cells on the chip source
`space` = 1	denotes conductor regions without holes in `geometrymask`
`nospace` = 0	denotes mssing conductor without holes in `geometrymask`
`hole` = -2	denotes holes in `geometrymask`
`nohole` = 0	denotes regions without holes in `holemask` (connected holeregions in `holemask` are represented by natural numbers)
`nocurrent` = Inf	denotes no current boundary condition in `currentmask` and `general_currentmask`
`general_current_1`	denote the boundary condition regions in `currentmask`
`general_current_1`	and `general_currentmask`